RESEARCH ARTICLE

N-WASP-Arp2/3 signaling controls multiple steps of dendrite maturation in Purkinje cells *in vivo*

Koichi Hasegawa, Takeshi K. Matsui, Junpei Kondo and Ken-ichiro Kuwako*

ABSTRACT

During neural development, the actin filament network must be precisely regulated to form elaborate neurite structures. N-WASP tightly controls actin polymerization dynamics by activating an actin nucleator Arp2/3. However, the importance of N-WASP-Arp2/3 signaling in the assembly of neurite architecture *in vivo* has not been clarified. Here, we demonstrate that N-WASP-Arp2/3 signaling plays a crucial role in the maturation of cerebellar Purkinje cell (PC) dendrites *in vivo* in mice. N-WASP was expressed and activated in developing PCs. Inhibition of Arp2/3 and N-WASP from the beginning of dendrite formation severely disrupted the establishment of a single stem dendrite, which is a characteristic basic structure of PC dendrites. Inhibition of Arp2/3 after stem dendrite formation resulted in hypoplasia of the PC dendritic tree. Cdc42, an upstream activator of N-WASP, is required for N-WASP-Arp2/3 signaling-mediated PC dendrite maturation. In addition, overactivation of N-WASP is also detrimental to dendrite formation in PCs. These findings reveal that proper activation of N-WASP-Arp2/3 signaling is crucial for multiple steps of PC dendrite maturation *in vivo*.

KEY WORDS: N-WASP, Arp2/3, Actin, Purkinje cell, Dendrite, Maturation, Mouse

INTRODUCTION

Brain function thoroughly relies on the sophisticated architecture of neural networks (Luo, 2021). The precise spatial configuration of axons and dendrites is assembled through the orchestration of intrinsic and extrinsic signals during development, and this process is imperative to establish functional neural circuits (Hasegawa and Kuwako, 2022).

Purkinje cells (PCs) in the cerebellum form the most elaborate dendritic trees in the vertebrate brain and have been an excellent model for studying dendrite development. PCs construct their dendritic arbors via consecutive dynamic remodeling during postnatal cerebellar development (Sotelo and Dusart, 2009) (Fig. 7). After migrating to the cerebellar cortex during the embryonic stage, PCs show a bipolar 'fusiform cell' shape with a few apical primitive dendrites until around postnatal day (P) 0. Subsequently, PCs retract apical dendrites, then continuously elongate and retract protrusions emerging from the cell body and display the 'stellate cell' shape, with numerous disoriented perisomatic dendrites by P4 (Armengol and Sotelo, 1991). After

Department of Neural and Muscular Physiology, School of Medicine, Shimane University, 89-1 Enya-cho, Izumo-shi, Shimane 693-8501, Japan.

*Author for correspondence (kuwako@med.shimane-u.ac.jp)

K.-i.K., 0000-0002-1380-3035

the stellate cell stage, PCs dramatically change their dendritic structure to one with a single apical stem dendrite, which is a basis for ultimate dendritic form, entering the 'young PC' stage by P10. A stem dendrite then begins to rapidly elongate and extensively branch into the molecular layer to establish a highly elaborate fan-shaped dendritic tree by P21 (Weiss and Pysh, 1978). Therefore, the maturation process of the PC dendrite can be divided into two major phases: the early phase, establishing the basic PC structure with a single stem dendrite, that lasts 12-13 days from the end of migration to the young PC stage; and the late phase, dramatically expanding dendrites to establish the final form of the dendritic tree for 2-3 weeks after young PC stage (Fig. 7).

A great number of molecules and signaling pathways have been found to be involved in PC dendrite formation *in vivo*; however, most of them are related to the machineries in the late phase of dendritic maturation, including the elongation, branching and spatial configuration of dendrites. These include the α2δ-2 voltage-dependent Ca^{2+} channel accessory subunit (Brodbeck et al., 2002), lysyl oxidase (Li et al., 2010), tissue plasminogen activator (Li et al., 2013), a chromatin remodeling factor Snf2h (also known as Smarca5; Alvarez-Saavedra et al., 2014), a GTPase Drp1 (Dnm1l; Fukumitsu et al., 2016), a serine/threonine kinase PDK1 (Liu et al., 2020), a vascular signaling angiopoietin Tie2 (Tek; Luck et al., 2021) for dendritic elongation and/or branching, a neurotrophin signaling neurotrophin 3 (NT-3; Ntf3)-tropomyosin-related kinase C (TrkC; Ntrk3) (Joo et al., 2014) and a synapse organizer GluD2 (Grid2)-Cbln1 (Takeo et al., 2021) for dendritic arbor size control, an adhesion molecule Pcdhγ (Lefebvre et al., 2012), a chemorepulsive signaling Slit2-Robo2 (Gibson et al., 2014), a kinase signaling LKB1 (Stk11)-SIK1/2 (Kuwako and Okano, 2018), an I-BAR superfamily protein MTSS1 (Kawabata Galbraith et al., 2018) for non-overlapping dendrite construction, and a cytoskeletal molecule β-III spectrin (Gao et al., 2011) for monoplanar dendritic spacing. In contrast, only a few molecules, including thyroid hormone 3,3′,5-triiodo-L-thyronine (T3) (Vincent et al., 1982; Legrand, 1984) and its downstream molecules retinoid-related orphan receptor alpha (RORα) (Landis and Sidman, 1978; Soha and Herrup, 1995; Boukhtouche et al., 2006; Takeo et al., 2015) and peroxisome proliferator-activated receptor gamma co-activator-1α (PGC-1α; Ppargc1a) (Hatsukano et al., 2017), have been identified to be involved in the early phase of dendritic maturation in PCs. Therefore, the molecular mechanisms that establish a single stem dendrite, which is the basis for the elaborate dendritic structure of PC, remain largely unknown.

Neural Wiskott-Aldrich Syndrome Protein (N-WASP) is a crucial regulator implicated in actin polymerization via the specific activation of an actin nucleator Arp2/3 complex (hereafter referred to as Arp2/3), a stable assembly of seven subunits including two actin-related proteins [Arp2 (Actr2) and Arp3 (Actr3)]. Arp2/3 generates branched actin networks by adding a monomer actin to an

existing actin filament on the c-terminal domain of the activated N-WASP at the juxtamembrane region (Pollard and Borisy, 2003). The N-WASP-Arp2/3-mediated *de novo* polymerization of branched actin filaments drives the protrusion of the plasma membrane, thereby prominently contributing to regulating neural structures such as growth cone and dendritic spine (Kessels et al., 2011; Konietzny et al., 2017). Previous studies using cultured hippocampal neurons and neuronal cell lines, such as N1E-115 and PC12 cells, have demonstrated that N-WASP and Arp2/3 control growth cone motility, spine formation, axonal and dendritic elongation, and branching (Irie and Yamaguchi, 2002; Strasser et al., 2004; Kakimoto et al., 2006; Pinyol et al., 2007; Korobova and Svitkina, 2008; Wegner et al., 2008; Dharmalingam et al., 2009; Chacón et al., 2012; Zhang et al., 2017). In addition, the nervous system-specific ablation of *N-WASP* (*Wasl*) or *Arpc2* (encoding Arp2/3 complex subunit Arpc2) genes severely impairs corticogenesis in mice, probably through the abnormalities in ciliogenesis of ependymal cells or migration of neural precursor cells (Jain et al., 2014; Wang et al., 2016). However, the importance of the N-WASP-Arp2/3 signaling in the formation of dendritic or axonal structures in the mammalian brain has never been elucidated. Recently, Arp2/3 was found to be required to initiate dendrite branchlet formation *in vivo* in *Drosophila* larva sensory neurons (Stürner et al., 2019). Therefore, the N-WASP-Arp2/3 signaling in mammalian nervous system may also have pivotal roles in the assembly of elaborate neurite architectures.

In this study, we provide evidence that N-WASP-Arp2/3 signaling in PCs is essential to establish a single stem dendrite in the early phase of dendritic maturation and to the assembly of an elaborate dendritic tree in the late phase. These findings reveal an essential role for the N-WASP-Arp2/3 signaling-mediated actin dynamics regulation in dendritogenesis *in vivo*.

RESULTS
N-WASP is expressed and activated in developing PCs
To explore functions of N-WASP-Arp2/3 signaling in neurite development *in vivo*, we focused on the dendritic maturation of PCs in the cerebellum. We first examined the expression of the molecules in N-WASP-Arp2/3 signaling in developing PCs using immunohistochemistry. At P6, when PCs are constructing a stem dendrite, N-WASP was highly expressed in the cell body of PCs with multiple perisomatic dendrites (Fig. 1A; Fig. S1A). Tyrosine 253 phosphorylation is crucial for N-WASP to release its autoinhibitory structure and subsequently activate Arp2/3 (Suetsugu et al., 2002). Using a specific antibody against phosphorylated N-WASP that detects tyrosine 253 phosphorylation, N-WASP was found to be highly activated at P6 (Fig. 1A; Fig. S1A). In addition to N-WASP, its target Arp2/3 and upstream regulator Cdc42 were also expressed in the cell body of P6 PCs (Fig. 1A; Fig. S1A). At P14, when PCs have already established a single stem dendrite and are actively extending and branching their dendrites, N-WASP, in addition to Arp2/3 and Cdc42, were clearly localized in the dendrites (Fig. 1B; Fig. S1B). Activated N-WASP was also localized in the P14 PC dendrites (Fig. 1B; Fig. S1B). These results indicate that N-WASP-Arp2/3 signaling may have roles in developing PCs.

N-WASP-Arp2/3 signaling is involved in dendrite development of PCs *in vitro*
The expression and activation of N-WASP in developing PCs prompted us to investigate the function of N-WASP-Arp2/3 signaling in dendrite development. Because Arp2/3 is involved in

the initiation of dendrite branchlet formation in invertebrate neurons (Stürner et al., 2019), we used time-lapse imaging to examine the spatiotemporal dynamics of Arp2/3 in the elongating and branching dendrites of cultured PCs. To analyze the localization of Arp2/3 in the dendrites of growing PCs, mCherry-tagged Arp3 (Arp3-mCherry) was co-transfected with green fluorescent protein (GFP) that was expressed under the PC-specific *L7* promoter (Fig. 2A,B). Live-cell imaging revealed that Arp3-mCherry accumulated very frequently at branching sites before the onset of *de novo* dendritic protrusion (Movies 1-3). The intensity of mCherry fluorescence signal was increased in 96.2% of the examined branching sites compared with the basal level, with over 15% fluorescence increase in 74.7% of the sites and over 30% increase in 30.4% of the sites (Fig. 2C). Arp3-mCherry was also abundantly localized in the growth cones of newly branched dendrites (Fig. 2B). These results suggest that Arp2/3 is dynamically recruited to local sites involved in dendritic branching and elongation.

Next, we used a pharmacological approach with specific inhibitors to examine whether N-WASP-Arp2/3 signaling is required for dendrite formation in PCs. When treated with wiskostatin, a selective inhibitor of N-WASP (Peterson et al., 2004; Ganeshan et al., 2006; King et al., 2011; Serrano-Pertierra et al., 2012), for prolonged periods of time, PCs showed marked reductions in dendrite length, branch number and area at 21 days *in vitro* (DIV) (Fig. 2D-G). In addition, prolonged treatment with CK-666 (Nolen et al., 2009) or ML-141 (Surviladze et al., 2010), specific inhibitors of Arp2/3 or Cdc42, also significantly reduced PC dendrite length, branching number, and area (Fig. 2D-G). Treatment with these inhibitors had no adverse effects on PC health (Fig. 2H). These results indicate that N-WASP-Arp2/3 signaling plays a pivotal role in establishing PC dendrites *in vitro*.

N-WASP-Arp2/3 signaling plays an essential role in the early phase of PC dendrite maturation *in vivo*
We next examined the role of N-WASP-Arp2/3 signaling during PC dendrite maturation *in vivo*. To this end, the previously characterized dominant-negative mutants of N-WASP that strongly inhibit the functions of endogenous Arp2/3 or N-WASP were introduced into the developing PCs. N-WASP is composed of several functional domains, including the WASP homology 1/Ena-VASP homology 1 domain that binds to the WASP-interacting protein family proteins, the basic domain that binds to phosphatidylinositol-(4,5)-biphosphate (PIP2), the GTPase-binding domain (GBD) that binds to Cdc42, the proline-rich domain (PRD) that binds to the BAR-domain proteins, and C-terminal domains (Miki et al., 1996; Kurisu and Takenawa, 2009) (Fig. 3A). The C-terminal domains of N-WASP contain the verprolin-homology domain (V) that binds to monomeric actin and the central (C) and acidic (A) domains that bind to Arp2/3. In a basal state, N-WASP is autoinhibited via the interaction between the GBD and C-terminal VCA domain. The competitive binding of the membrane-anchored Cdc42 to GBD recruits N-WASP to the plasma membrane and induces its activation by releasing it from the autoinhibitory structure. PIP2 that is abundant in the plasma membrane also recruits and activates N-WASP synergistically with Cdc42. Although the VCA domain interacts with Arp2/3 and activates Arp2/3-mediated actin polymerization, the VCA fragment of N-WASP (N-WASP VCA) lacks all other domains including the basic domain and GBD. Therefore, N-WASP VCA fails to localize at the plasma membrane (Fig. S2) and sequesters Arp2/3 in the cytoplasm (Machesky and Insall, 1998), serving as a
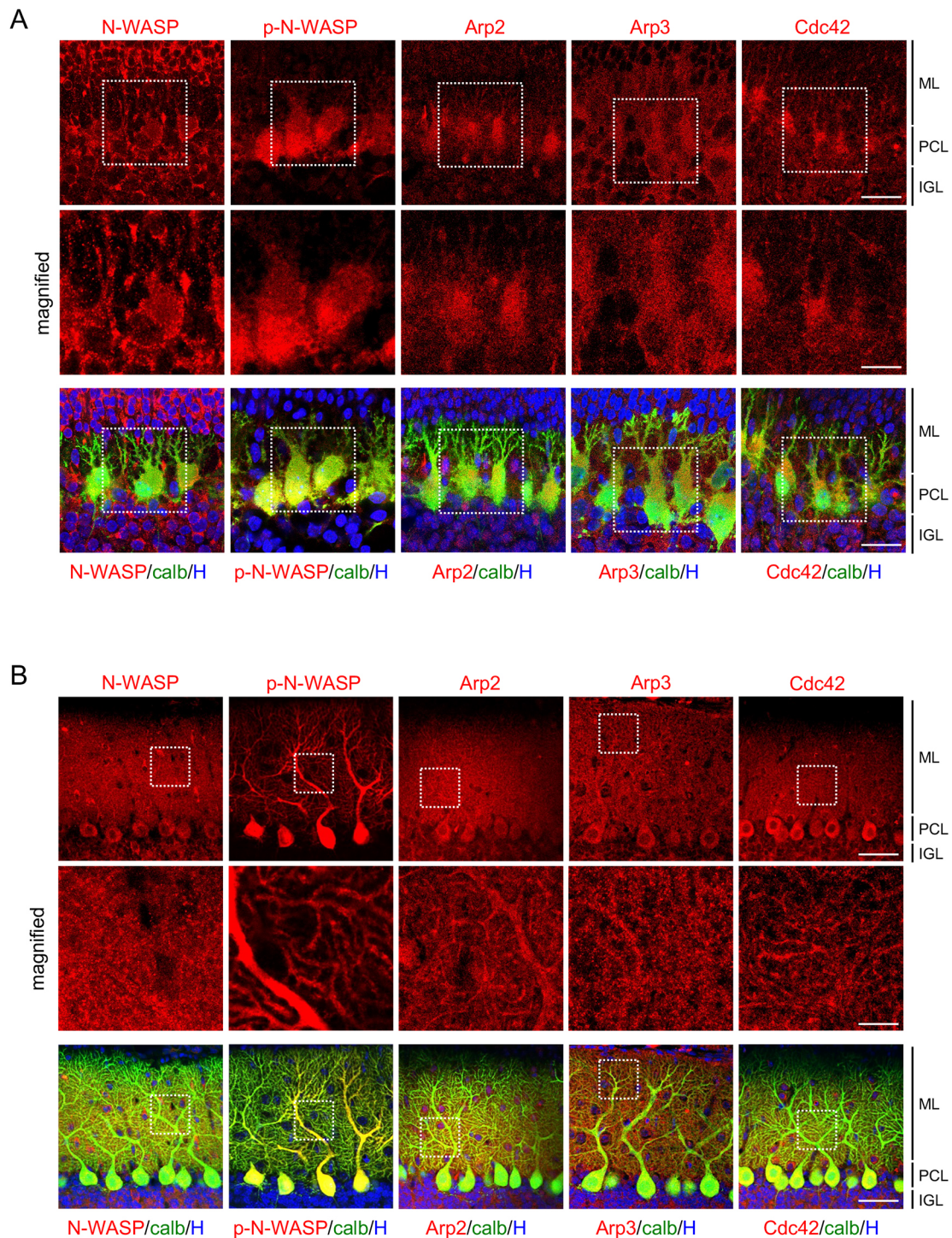
DEVELOPMENT

Fig. 1. N-WASP-Arp2/3 signaling molecules are expressed in developing PCs. (A,B) Sections of P6 (A) and P14 (B) cerebella were co-immunostained with antibodies against calbindin (calb, a PC marker) and N-WASP/phospho-N-WASP (p-N-WASP)/Arp2/Arp3/Cdc42. Dotted boxes in the top and bottom panels are magnified in middle panels. Note that N-WASP, p-N-WASP, Arp2, Arp3 and Cdc42 are expressed in the cell body and dendrites at P6 and P14 in PCs. H, Hoechst; IGL, internal granule cell layer; ML, molecular layer; PCL, Purkinje cell layer. Scale bars: 20 µm (top and bottom panels in A); 10 µm (middle panels in A and B); 50 µm (top and bottom panels in B).

dominant-negative mutant that strongly inhibits the Arp2/3 function (Strasser et al., 2004; Wegner et al., 2008).

To analyze the role of the N-WASP-Arp2/3 signaling in the early phase of dendritic maturation of PCs, N-WASP VCA was specifically expressed in PCs using an *in utero* electroporation method (Kuwako and Okano, 2018). In the postnatal stage, the majority of N-WASP VCA-expressing PCs were normally aligned in the Purkinje cell layer (PCL), even though a very small fraction of PCs was ectopically localized in the granule cell layer and white matter probably due to migration defect. To avoid non-cell autonomous effects caused by abnormal PC location on dendrite development, we analyzed only the PCs in the PCL. At P21, when
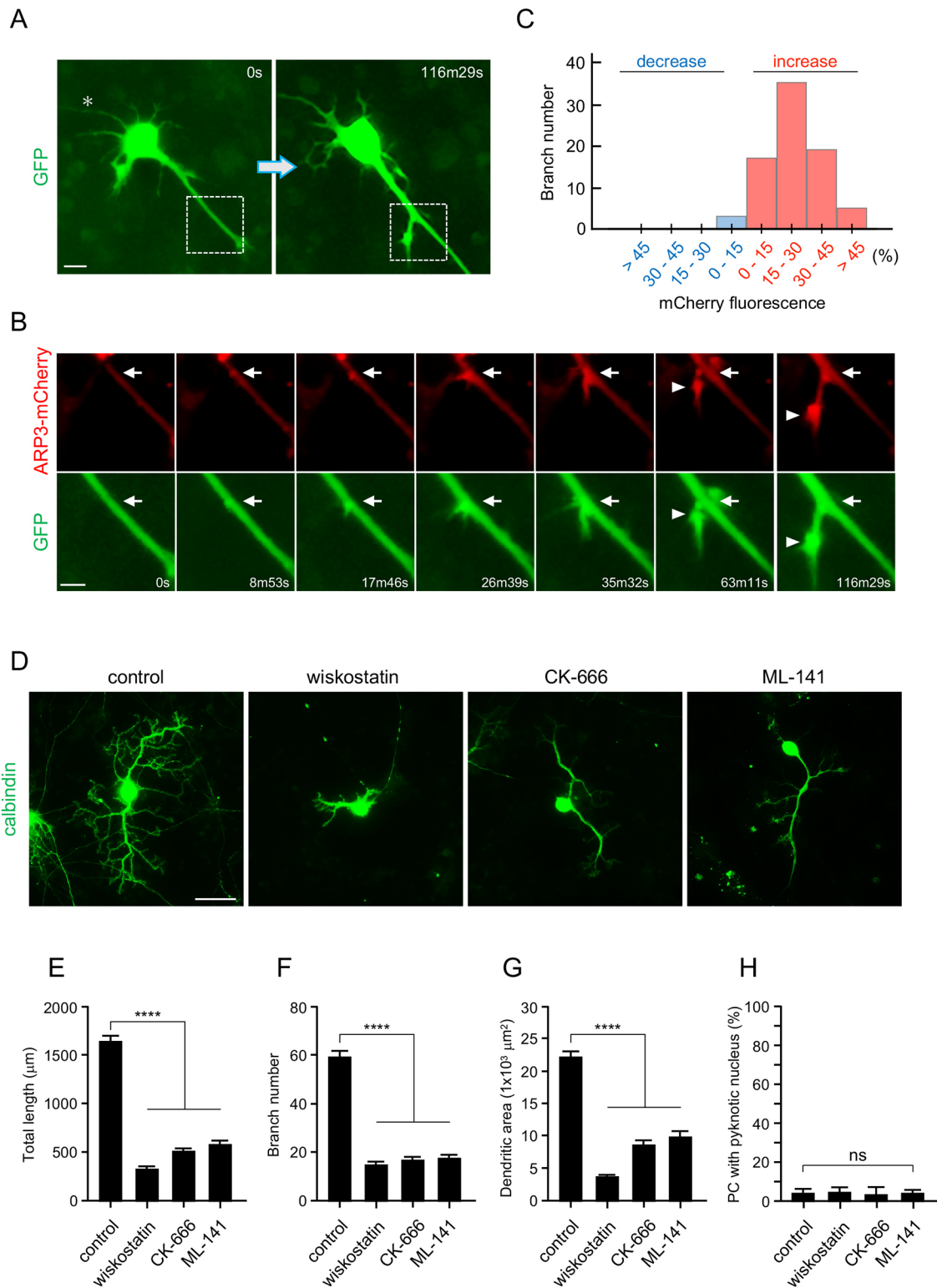
Fig. 2. See next page for legend.

mature dendrites had just developed in the control PCs (Weiss and Pysh, 1978), N-WASP VCA-expressing PCs exhibited severely stunted growth of dendrites (Fig. 3B,C). The dendrites of N-WASP VCA-expressing PCs were significantly reduced to 12.9%, 13.2% and 15.0% in length, branch number and area, respectively, compared with control PCs (Fig. 3D-F). The forced expression of

PRDVCA fragment (Pinyol et al., 2007), which, like N-WASP VCA, is unable to localize to the plasma membrane (Fig. S2), also greatly reduced PC dendrites to 9.4%, 9.7% and 11.9% in length, branch number and area, respectively, compared with control PCs (Fig. 3A,B,D-F). On the other hand, the branching frequency of dendrites did not differ between VCA- or PRDVCA-expressing PCs

Fig. 2. N-WASP-Arp2/3 signaling is involved in dendrite development in cultured PCs. (A-C) Live cell imaging analysis for dendrite branching and Arp3 localization in cultured PCs. *L7* promoter-driven GFP and *CAG* promoter-driven Arp3-mCherry were co-expressed in PCs at 0 DIV. The initial and final GFP images of a time-lapse series of a PC at 5 DIV are shown in A. Magnified time-lapse images of the region in the dotted box in A are presented in B. Arrows and arrowheads indicate the site of the new dendritic branch and dendritic growth cone, respectively. Note that Arp3-mCherry accumulated in the site of *de novo* dendritic protrusion before its initiation and in the growth cone of newly branched dendrite. Quantification of the number of branch sites that exhibit the increase or decrease of mCherry-fluorescence intensity at the time point just before branching is shown in C. In total, 79 branches from 51 PCs were analyzed. Higher fluorescence signal was observed in 76 of the 79 branches, whereas only three branches showed a decrease in fluorescence signal, and this was a weak decrease (0-15% decrease). (D) Inhibitor experiments *in vitro*. PCs cultured with N-WASP inhibitor wiskostatin (1 μM), Arp2/3 inhibitor CK-666 (50 μM) or Cdc42 inhibitor ML-141 (10 μM) for 21 days were immunostained with antibody against calbindin. (E-H) Quantification of total dendrite length (E), branch number (F), dendrite area (G) and percentage of PC with pyknotic nucleus (H) at 21 DIV in the experiment shown in D. The data represent the mean±s.e.m. n=74 cells (control), n=77 cells (wiskostatin), n=74 cells (CK-666) and n=74 cells (ML-141) in (E-G). n=3 experiments (40-55 cells were quantified in each experiment) for all conditions in (H). ****P<0.0001 (non-repeated one-way ANOVA with a post hoc Bonferroni correction). Ns, not significant. Scale bars: 10 μm (A); 5 μm (B); 50 μm (D).

and control PCs (Fig. 3G). Consistent with the putative mechanism of these dominant-negative mutants, in which endogenous Arp2/3 is unable to localize at the juxtamembrane regions leading to loss of function, the membrane-anchored forms of N-WASP VCA or PRDVCA significantly attenuated the effects of the VCA or PRDVCA fragment on PC dendrite development (Fig. 3B,D-F). The N-WASP VCA or PRDVCA-expressing PCs at P21 extended multiple perisomatic dendrites and did not possess an apparent stem dendrite in most cases, whereas control PCs have a single apical stem dendrite (Fig. 3C). Because these dendritic morphologies of VCA- or PRDVCA-expressing PCs are strongly reminiscent of the shape of immature PCs during development, we quantified the orientation and number of dendrites. Developing PCs showed drastic morphological changes of their dendrites during the early postnatal stage (Sotelo and Dusart, 2009). Postmigratory PCs first showed bipolar 'fusiform' shape at ∼P0 followed by the 'stellate cell' shape with multidirectional perisomatic dendrites at ∼P4 (Fig. 3H; Fig. 7; Fig. S3A). Thereafter, by P10, PCs rapidly retract basal and lateral dendrites and reduce number of dendrites to become a polarized 'young PC' shape, which has a single stem dendrite extending toward the molecular layer (Fig. 3H,I; Fig. 7; Fig. S3A). However, the orientation and number of dendrites of N-WASP VCA or PRDVCA-expressing PCs at P21 are similar to that of control PCs transitioning from the satellite cell stage to young PC stage at P6-P8, (Fig. 3H,I), suggesting that inhibiting Arp2/3 function halts the progression of PC dendrite maturation just after the stellate cell stage. In addition, a few N-WASP VCA or PRDVCA-expressing PCs had relatively elongated stem-like dendrites, but most of them showed aberrant hypertrophic structures with abnormal accumulation of the Golgi apparatus (Fig. S4). We next analyzed the involvement of N-WASP as an upstream regulator in the Arp2/3-mediated dendritic maturation of PCs *in vivo* using another dominant-negative mutant of N-WASP that lacks the VCA domain (N-WASP ΔVCA) (Fig. 3A) (Pinyol et al., 2007; Wegner et al., 2008). The membrane-anchored form of N-WASP ΔVCA (mem ΔVCA) can occupy its activators at the plasma membrane, such as Cdc42 and PIP2, but fails to interact with Arp2/3, thereby preventing endogenous N-WASP from activating

Arp2/3. We found that N-WASP mem ΔVCA-expressing PCs at P21 have numerous multidirectional perisomatic dendrites that are similar to the dendrites of N-WASP VCA or PRDVCA-expressing PCs (Fig. 3J; Fig. S5), suggesting that N-WASP is essential to the machinery of Arp2/3-mediated dendritic maturation in PCs. N-WASP PRDVCA or mem ΔVCA-expressing PCs at P35 showed similar dendritic abnormalities to those at P21 (Figs S3B and S5B), suggesting that inhibition of N-WASP-Arp2/3 signaling causes arrest, but not delay, of dendritic maturation after stellate cell stage. We then probed whether Cdc42, a major activator of N-WASP, was involved in the N-WASP-Arp2/3-mediated dendritic maturation in PCs using a rescue experiment. The defects in length, branch number and area of PC dendrites caused by the expression of N-WASP VCA were largely rescued by co-expression of mCherry-tagged wild-type N-WASP (Fig. 4A-D), supporting the fact that N-WASP is a crucial upstream regulator of Arp2/3 in this context. However, co-expression of mCherry-tagged N-WASP H208D mutant, in which the histidine residue at 208 in the GBD was substituted with aspartic acid, abolishing the Cdc42-binding to N-WASP (Miki et al., 1998; Rohatgi et al., 1999), completely failed to rescue the defects caused by the expression of N-WASP VCA (Fig. 4A-D). This result suggests that Cdc42 is indispensable for eliciting the N-WASP-Arp2/3-mediated maturation of PC dendrites. Taken together, these results indicate that the Cdc42-N-WASP-Arp2/3 signaling plays an essential role in the early phase of PC dendrite maturation, particularly in the establishment of an apical stem dendrite.

Arp2/3 signaling plays an essential role in the late phase of PC dendrite maturation *in vivo*

We further investigated whether N-WASP-Arp2/3 signaling was involved in the late phase of dendrite maturation in PCs. To this end, N-WASP PRDVCA was specifically expressed in PCs under the *L7* promoter using the adeno-associated virus (AAV) vector after the establishment of a single stem dendrite. We intravenously injected N-WASP PRDVCA-expressing AAV at P7 and detected its expression in PCs from P10 (Fig. 5A; Fig. S6). The expression of N-WASP PRDVCA in PCs during the late phase of dendrite maturation resulted in the significantly attenuated growth of the dendritic tree at P21 (Fig. 5B). The dendrites of PCs that expressed N-WASP PRDVCA from the young PC stage were significantly reduced to 40.7% in length, 36.9% in branch number and 50.9% in area compared with control PCs (Fig. 5D-F). The branching frequency of dendrites was also decreased in N-WASP PRDVCA-expressing PCs (Fig. 5G). In addition, abnormal hypertrophic structures were frequently observed in the stem dendrites of PCs expressing N-WASP PRDVCA (Fig. 5B,C), similar to some PCs expressing N-WASP VCA or PRDVCA through *in utero* electroporation (Fig. S4). These results strongly indicate that N-WASP-Arp2/3 signaling also plays an essential role in the machineries for elongation and branching of PC dendrites during the late phase of dendrite maturation.

Proper activation level of N-WASP-Arp2/3 signaling is required for PC dendrite development *in vivo*

We also investigated whether overactivation of N-WASP influences the development of PC dendrites. We first overexpressed wild-type N-WASP in PCs through *in utero* electroporation, and found that those PCs normally developed an intricate dendritic tree without any apparent defects at P21 (Fig. S7A). This observation indicates that the upstream activation machinery for N-WASP, which is likely to be mediated by Cdc42 (Fig. 4), is limited in the physiological
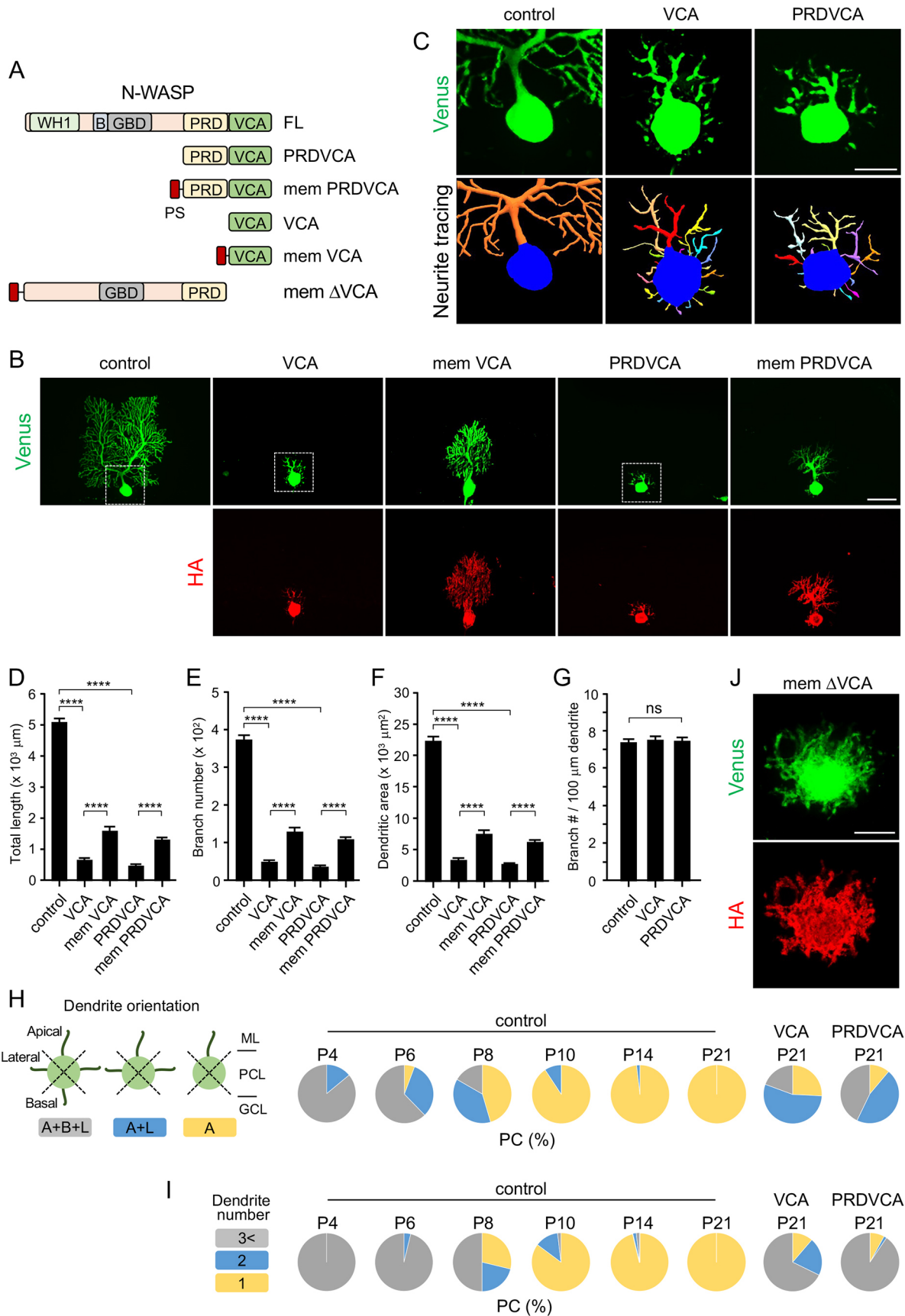
Fig. 3. See next page for legend.

Fig. 3. N-WASP-Arp2/3 signaling is essential for the early phase of dendritic maturation in PCs *in vivo*. (A) Schematic of N-WASP mutants used in the experiments shown in (B-I). WH1, WASP homology domain 1; B, basic domain; GBD, GTPase-binding domain; PRD, proline-rich domain; VCA, verprolin-homology, central and acidic domains; PS, palmitoylation signal; mem, membrane-anchored. (B) *Z*-sections of control, VCA, mem VCA, PRDVCA and mem PRDVCA-expressing PCs at P21. HA-tagged N-WASP mutants were specifically expressed in PCs through *in utero* electroporation. Venus was co-expressed in PCs in all conditions to visualize dendrite morphology. Sections were immunostained with antibodies against GFP (for Venus) and HA. Dotted boxes indicate the positions of the high-magnification images shown in C. (C) High-magnification images of Venus-expressing cells in B. Bottom panels represent neurite reconstruction of a PC using Neurolucida. (D-G) Quantification of total dendrite length (D), branch number (E), dendrite area (F) and branching frequency (G) at P21 in the experiment shown in B. The data represent the mean±s.e.m. *n*=35 cells (control), *n*=38 cells (VCA), *n*=30 cells (mem VCA), *n*=42 cells (PRDVCA) and *n*=31 cells (mem PRDVCA) from 3-5 mice. ****$P<0.0001$ (non-repeated one-way ANOVA with a post hoc Bonferroni correction). ns, not significant. (H,I) Quantification of orientation (H) and number (I) of perisomatic dendrites in Venus-expressing control PCs between P4 and P21, and VCA or PRDVCA (with Venus)-expressing PCs at P21. In total, 50 (control P4), 53 (control P6), 66 (control P8), 54 (control P10), 54 (control P14), 66 (control P21), 62 (N-WASP VCA P21) and 63 (N-WASP PRDVCA P21) cells were analyzed, and the proportions of PCs are shown. To quantify dendrite orientation in H, PCs were divided into the following three groups: A+B+L, PC with dendrites extending toward all directions (apical, basal and lateral directions); A+L, PC with dendrites extending toward apical and lateral directions); A, PC with dendrite(s) extending toward only apical direction. ML, molecular layer; PCL, Purkinje cell layer; GCL, granule cell layer. (J) Section of N-WASP mem ΔVCA and Venus-expressing PC at P21. HA-tagged N-WASP mem ΔVCA and Venus were co-expressed in PCs by *in utero* electroporation. Section was immunostained with antibodies against GFP (for Venus) and HA. Note that N-WASP mem ΔVCA-expressing PC possesses many multidirectional perisomatic dendrites without a stem dendrite. Scale bars: 50 μm (B); 20 μm (C,J).

condition in PCs. We then expressed a constitutively-active form of N-WASP in PCs. N-WASP Y253E, in which the tyrosine residue at 253 was replaced by glutamic acid, is constitutively active because it mimicked the phosphorylation state and released N-WASP autoinhibition (Suetsugu et al., 2002). To increase the activation level of N-WASP, the membrane-anchored form of N-WASP Y253E (mem Y253E) was expressed in PCs (Fig. 6; Fig. S8). N-WASP mem Y253E-expressing PCs at P21 showed different dendritic phenotypes in different cells (Fig. 6A). Although, unlike N-WASP VCA- or PRDVCA-expressing PCs, many N-WASP mem Y253E-expressing PCs have a stem dendrite, the expression of N-WASP mem Y253E caused increased primary dendrite number in 31.7% of PCs, abnormal orientation in 23.4% and decreased dendritic height in 25.4% (Fig. 6B). In addition, overactivation of N-WASP by mem Y253E expression unexpectedly decreased the branching frequency of dendrites (Fig. 6C). This result indicates that an appropriate activation level of N-WASP is important for normal development of PCs.

DISCUSSION

Arp2/3 constitutes a common pathway to generate actin filaments in eukaryotes. Numerous *in vitro* studies have disclosed the functions of N-WASP-Arp2/3 signaling in neurite morphogenesis, including the regulation of the growth cone and dendritic spine; however, the bona fide role and importance of this signaling in neurite formation *in vivo* has not yet been described. The present study demonstrates the essential roles of N-WASP-Arp2/3 signaling in dendrite maturation in PCs *in vivo*, including the establishment of a single stem dendrite and the expansion of dendritic tree.

Roles of N-WASP-Arp2/3 signaling in PC dendrite maturation

Although analyses by exogenous expression of dominant-negative mutants generally involve concerns about nonspecific effects, the dominant-negative mutants of N-WASP-Arp2/3 signaling used in this study have been well established in a number of studies (Machesky and Insall, 1998; Miki et al., 1998; Rohatgi et al., 1999; Suetsugu et al., 2002; Strasser et al., 2004; Pinyol et al., 2007; Wegner et al., 2008) and overexpression of wild-type N-WASP or N-WASP Y253E without membrane-anchored signal did not affect PC dendrite development (Fig. S7A,B). Therefore, the dendritic phenotypes obtained by the forced expression of the dominant-negative mutants of N-WASP may represent the results of functional inhibition of N-WASP-Arp2/3 signaling. The PCs that expressed N-WASP VCA, PRDVCA or mem ΔVCA in the embryonic stage retained a stellate cell-like shape, but not a fusiform cell shape, even at P21 (Fig. 3; Fig. 7; Fig. S5A). Therefore, N-WASP-Arp2/3 signaling plays a crucial role in the formation of a stem dendrite, but not in the elimination of primitive dendrites of fusiform PCs during the early phase of dendrite maturation. In addition, inhibiting N-WASP-Arp2/3 signaling after the young PC stage caused abnormalities in the dendritic arbors at P21 (Fig. 5), suggesting that this signaling is also indispensable in dendritic elongation and branching during the late phase of dendrite maturation (Fig. 7). *De novo* polymerization of branched actin filaments in the dendritic growth cone and protrusion is likely to be the basis of the N-WASP-Arp2/3 signaling-mediated elongation and branching of PC dendrites during the late phase. Furthermore, overactivation of N-WASP-Arp2/3 signaling led to a moderately anomalous dendritic tree at P21 (Fig. 6), showing increased dendrite number, abnormal dendrite orientation and reduced dendrite size, indicating that maintaining an appropriate activation level of N-WASP-Arp2/3 signaling during the entire process of dendrite formation is essential for normal dendrite development in PCs.

Mechanisms establishing a single stem dendrite in PCs

After the stellate cell stage, PCs dynamically reorganized their dendritic structure to create a single stem dendrite in just 6 days between P4 and P10, which became the basis for the subsequent elongation and ramification into a highly branched fan-shaped dendritic tree (Fig. 7; Fig. S3A). However, the molecular mechanism for the formation of a single stem dendrite specifically on the apical side has not yet been elucidated. This process includes several sequential events that must involve cytoskeletal reorganization: (1) selective regression of dendrites emerging from the basal and lateral sides; (2) selective strengthening of a single dendrite among apical dendrites; (3) elimination of the remaining dendrites (Fig. 3H,I; Fig. S3A) (Sotelo and Dusart, 2009). During this developmental process between P4 and P10, most PCs that form a thick apical stem dendrite still have lateral dendrites; further development eliminates all but the stem dendrite (Fig. S3A), suggesting that the three events described above are sequential, with some degree of overlap.

The present study demonstrates that inhibition of N-WASP-Arp2/3 signaling severely impedes the formation of a single stem dendrite, but it remains unknown how this signaling functions in the process of a single stem dendrite formation. Accumulating evidence in cultured primary neurons demonstrates that N-WASP-Arp2/3 signaling plays pivotal roles in growth cone motility through the induction of lamellipodia and filopodia (Korobova and Svitkina, 2008; Chacón et al., 2012; San Miguel-Ruiz and Letourneau, 2014). We also observed the recruitment of Arp3 in the growth cone of
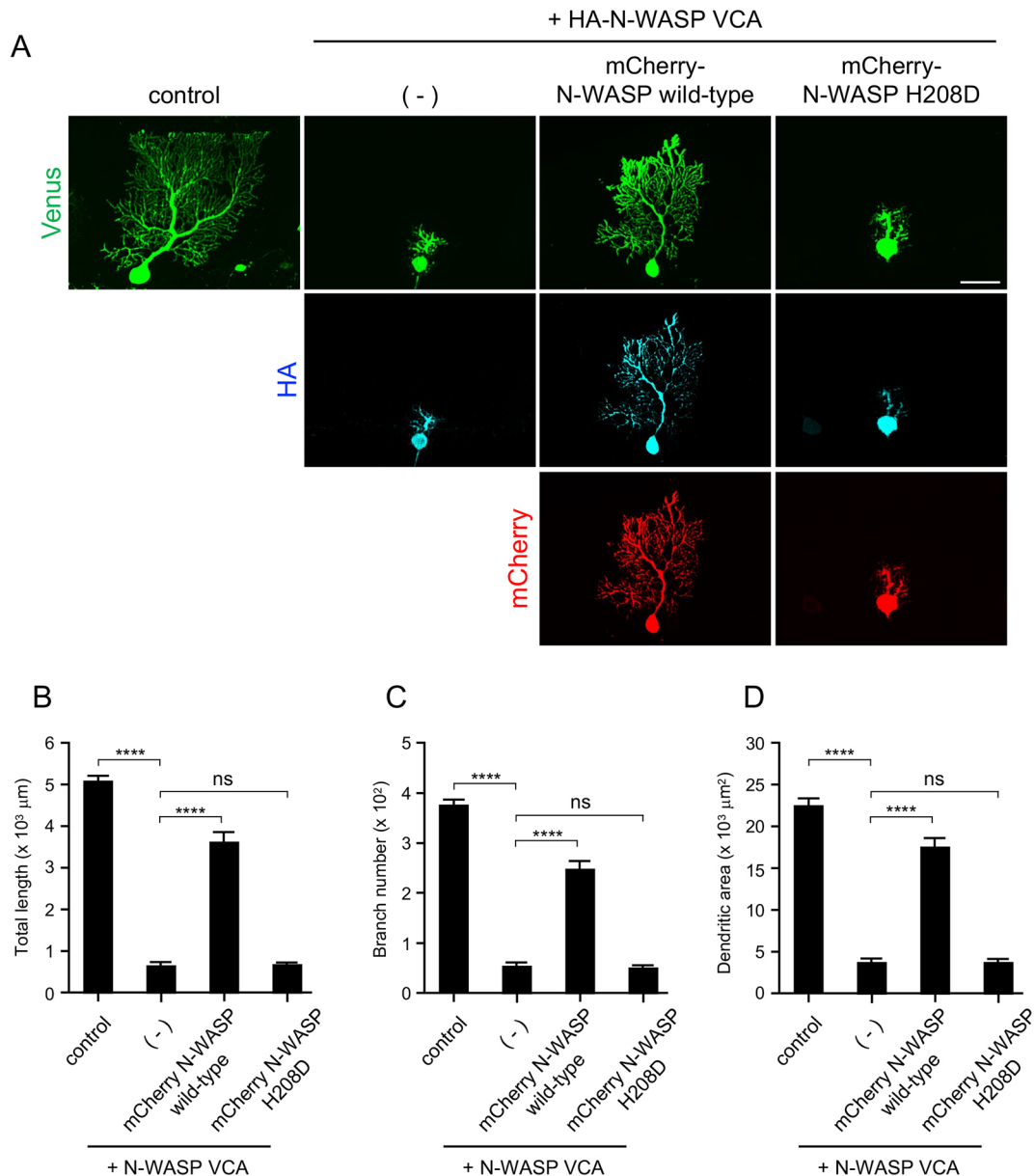
Fig. 4. Cdc42 regulates N-WASP-Arp2/3 signaling-mediated maturation of PC dendrites. (A) *Z*-sections of control, N-WASP VCA and mCherry-N-WASP wild-type or H208D-expressing PCs at P21. HA-tagged N-WASP VCA with or without mCherry-fused N-WASP wild-type or H208D were specifically expressed in PCs through *in utero* electroporation as the indicated combination. Venus was co-expressed in PCs under all conditions to visualize dendrite morphology. Sections were immunostained with antibodies against GFP (for Venus), RFP (for mCherry) and HA. (B-D) Quantification of total dendrite length (B), branch number (C) and dendrite area (D) at P21 in the experiment shown in A. The data represent the mean±s.e.m. *n*=35 cells (control), *n*=31 cells (VCA), *n*=34 cells (HA-NWASP VCA and mCherry-N-WASP wild-type) and *n*=33 cells (HA-NWASP VCA and mCherry-N-WASP H208D) from three mice. ****$P<0.0001$ (non-repeated one-way ANOVA with a post hoc Bonferroni correction). ns, not significant. Scale bar: 50 µm.

elongating PC dendrites (Fig. 2B; Movies 1-3). However, inhibiting N-WASP-Arp2/3 signaling promotes axonal elongation and branching, in apparent contradiction to the positive effect of this signaling on growth cone motility (Strasser et al., 2004; Kakimoto et al., 2006; Pinyol et al., 2007; Dharmalingam et al., 2009). Although this mechanism remains to be elucidated, the depletion of N-WASP-Arp2/3 signaling may trigger the extension of Arp2/3-independent parallel actin fibers in the growth cone periphery that accelerate axonal elongation (Kessels et al., 2011). In addition, the role of the N-WASP-Arp2/3 signaling in generating primary dendrites in cultured hippocampal neurons is controversial; some studies demonstrated an increase in primary dendrite number

(Pinyol et al., 2007; Zhang et al., 2017), some a decrease in number (Korobova and Svitkina, 2008), and some showed no effect (Dharmalingam et al., 2009). Thus, the functions and mechanisms of N-WASP-Arp2/3 signaling in the assembly of neurite structure are still ambiguous. In PCs, even if N-WASP-Arp2/3 signaling promotes or suppresses the protrusion of primary dendrites, it is hard to explain how this signaling leaves exactly one dendrite by regulating growth cone motility. The phenomenon of leaving a single stem dendrite among multiple dendrites is conserved in zebrafish and mice PCs, even though zebrafish PCs have diverse dendritic structures that differ from those of mice in many aspects including complexity and planarity (Tanabe et al., 2010). In
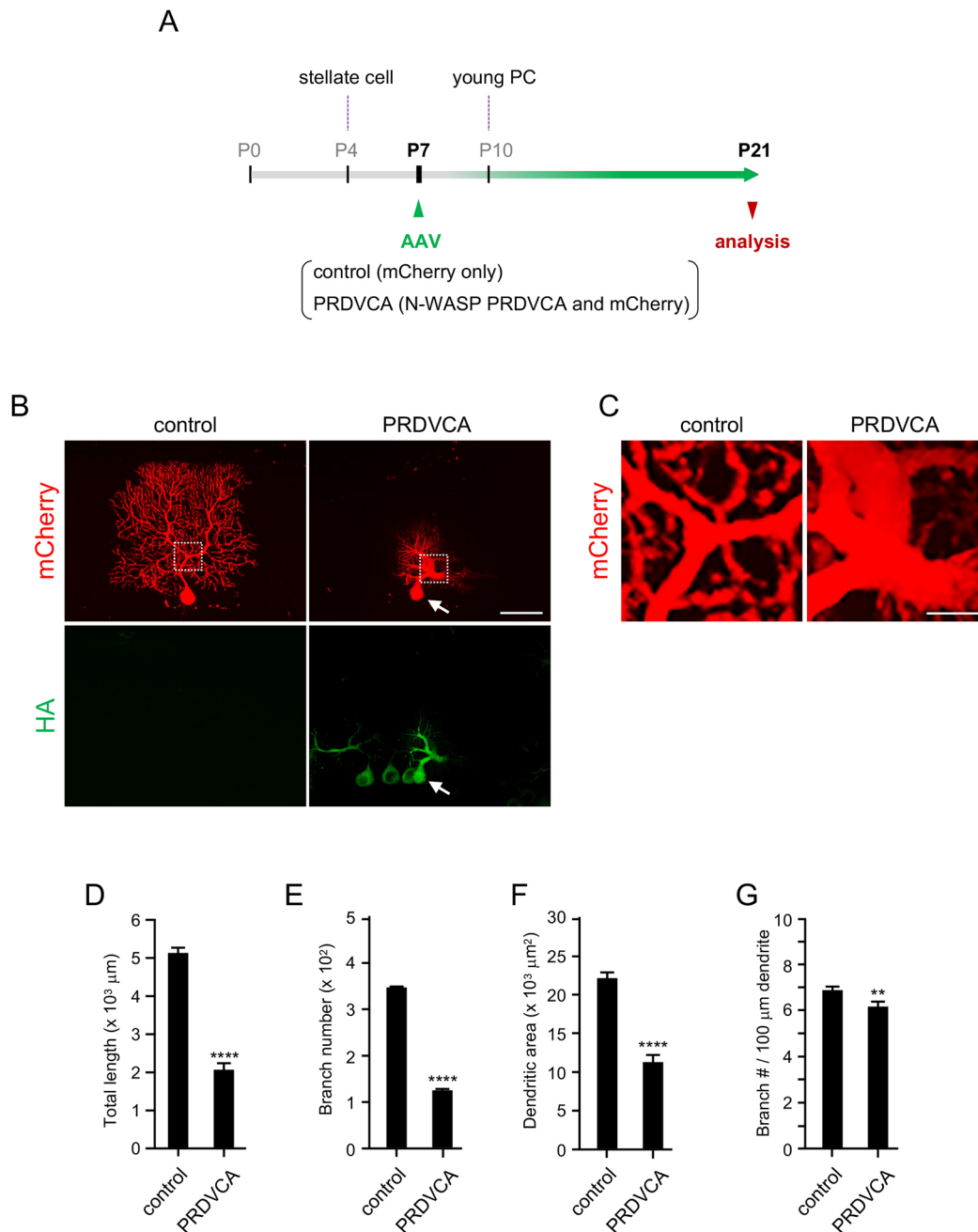
Fig. 5. N-WASP-Arp2/3 signaling is essential for the late phase of PC dendrite maturation *in vivo.* (A) Scheme of experiment using AAV-mediated gene transfer shown in B. HA-N-WASP PRDVCA-expressing AAV was intravenously injected at P7, and PCs were analyzed at P21. mCherry-expressing AAV was also injected to visualize dendrite morphology. (B,C) *Z*-sections of control and PRDVCA-expressing PCs at P21. Sections were co-immunostained with antibodies against RFP (for mCherry) and HA. The arrows in B indicate the PC that co-expresses HA-N-WASP PRDVCA and mCherry. The dotted boxes in B indicate the positions of high-magnification images shown in C. Note that hypertrophic structures were observed in the stem dendrite of PCs expressing N-WASP PRDVCA. (D-G) Quantification of total dendrite length (D), branch number (E), dendrite area (F) and branching frequency (G) in the experiment shown in B. The data represent the mean±s.e.m. *n*=35 cells (control) and *n*=30 cells (PRDVCA). ****$P<0.0001$, **$P<0.002$ (unpaired two-tailed Student's *t*-test). Scale bars: 50 µm.

zebrafish PCs, the specific accumulation of the Golgi apparatus at the base of one of several immature dendrites appears to determine that one as being the stem dendrite at the later stage (Tanabe et al., 2010). In mice, between the stellate cell and young PC stages, the PC nucleus is attached to the basal pole side, resulting in organelles including the Golgi apparatus being confined to the apical side of the cytoplasm (Larramendi, 1969). In addition, WASP-Arp2/3 signaling regulates the position of the Golgi apparatus in NIH3T3

cells (Magdalena et al., 2003). Therefore, N-WASP-Arp2/3 signaling in mouse PCs could possibly mediate a specific cellular accumulation of the Golgi apparatus, leading to the selection of one dendrite in the apical side for a future stem dendrite. Another possible mechanism for the Arp2/3-mediated selection of a single stem dendrite may involve the actin patch that is a specialized microstructure of actin. The actin patch is a few microns in diameter, and is rich in branched F-actin, providing a site for filopodia
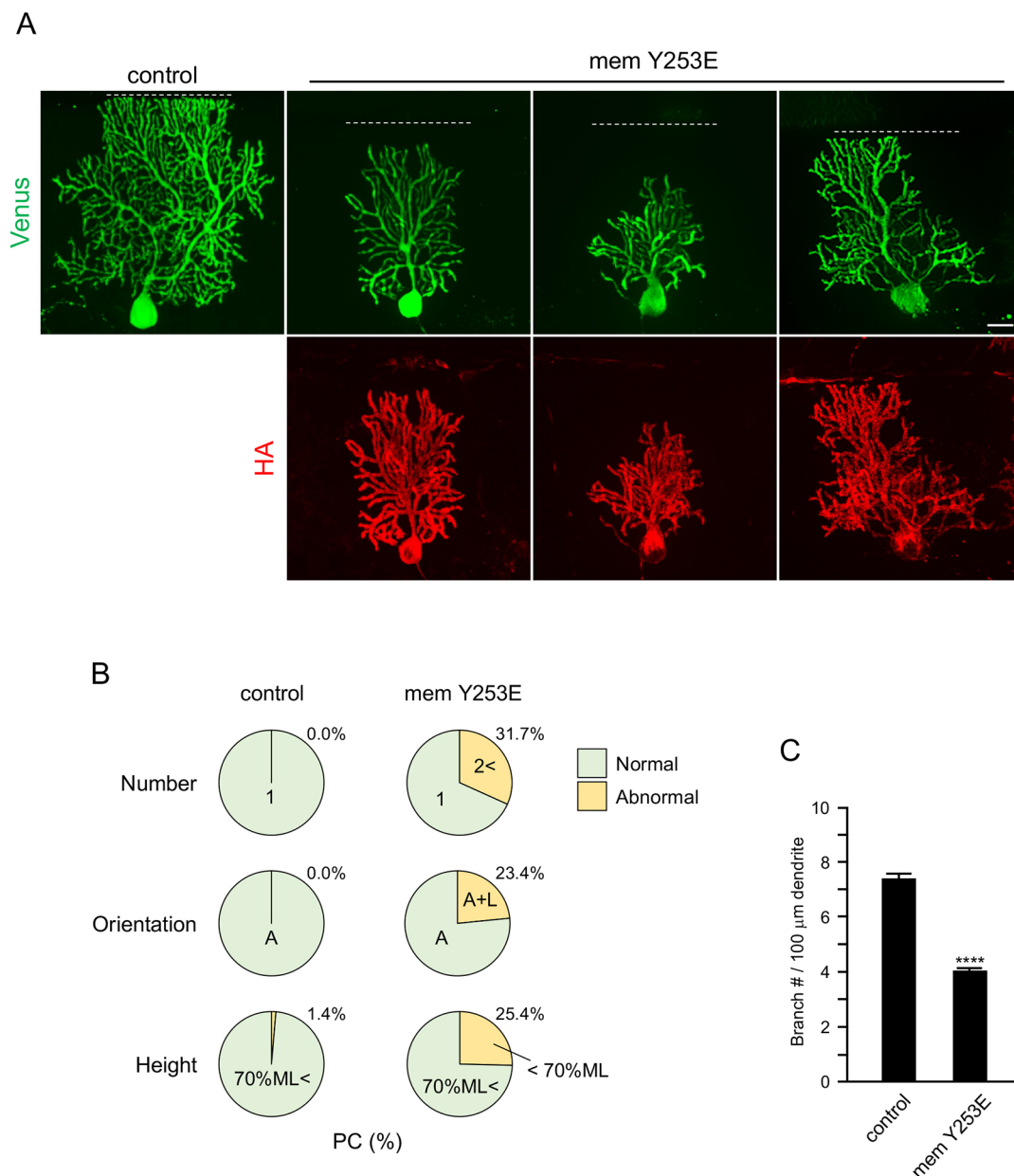
Fig. 6. Overactivation of N-WASP impairs development of PC dendrites. (A) Z-sections of control and membrane-anchored N-WASP Y253E (mem Y253E)-expressing PCs at P21. HA-tagged N-WASP mem Y253E was specifically expressed in PCs by *in utero* electroporation. Venus was expressed in PCs to visualize dendrite morphology. Sections were co-immunostained with antibodies against GFP (for Venus) and HA. Three examples of N-WASP Y253E-expressing PCs are shown. The dotted lines indicate the top of the molecular layer. (B) Quantification of number, orientation and height of dendrites in control and N-WASP mem Y253E-expressing PCs at P21 in the experiment shown in A. PCs were divided into the two groups, normal and abnormal, according to the following criteria: dendrite number [normal, one dendrite (1); abnormal, more than two dendrites (2<)], dendrite orientation [normal, apical only (A); abnormal, apical and lateral (A+L); see Fig. 3H] and dendritic height [normal, more than 70% height of the molecular layer (ML); abnormal, less than 70% height of the molecular layer]. A total of 84 (control, number), 63 (mem Y253E, number), 84 (control, orientation), 64 (mem Y253E, orientation), 74 (control, height) and 63 (mem Y253E, height) cells were analyzed and the proportions of PCs are shown. The numbers represent the percentage of abnormal PCs. (C) Quantification of the branching frequency at P21 in the experiment shown in A. The data represent the mean±s.e.m. *n*=35 cells (control) and *n*=32 cells (mem Y253E). ****$P<0.0001$ (unpaired two-tailed Student's *t*-test). Scale bar: 20 µm.

protrusion (Korobova and Svitkina, 2008; Willig et al., 2014). Furthermore, Arp2/3 is the only regulator for actin branching, and is involved in the formation of actin patches in neurons (Spillane et al., 2011, 2012). Thus, we could investigate the detailed cellular localization of the actin patch and Golgi apparatus between P4 and P10 in normal and N-WASP VCA- or mem ΔVCA-expressing PCs, and clarify their contribution to the determination of a single stem dendrite.

Given that the dendritic elimination after the stellate cell stage does not occur in PCs that have failed to form a stem dendrite (Fig. 3B,C,J; Figs S3B,C and S5), assigning a single apical dendrite to become a stem dendrite may serve as a trigger to activate the unknown mechanism that eliminates the remaining dendrites. A similar phenomenon is well-known in axon specification in differentiating hippocampal neurons; once one of several immature neurites is destined to become an axon, it triggers the differentiation
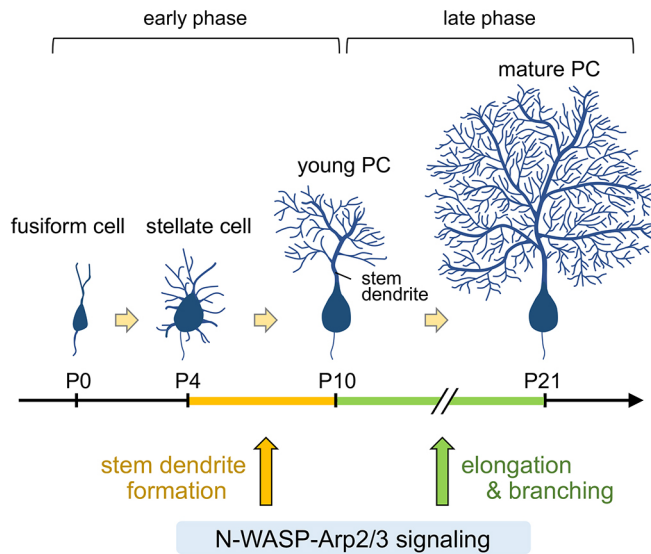
Fig. 7. Role of N-WASP-Arp2/3 signaling in PC dendrite maturation. During postnatal development, the PC dramatically changes its dendrite structure. The maturation process of PC dendrites is divided into two phases: early phase, in which a single stem dendrite is established, and late phase, in which dendrites rapidly expand. In the early phase, PCs progress from the fusiform cell stage to young PC stage with a single stem dendrite via the stellate cell stage. In the late phase, rapid elongation and extensive branching of dendrites construct a large fan-shaped dendritic tree. N-WASP-Arp2/3 signaling is essential for establishing a single stem dendrite and expanding the dendritic tree.

of the remaining neurites into dendrites, but not axons (Yoshimura et al., 2006). As N-WASP-Arp2/3 signaling is not involved in the machinery of actin depolymerization (Konietzny et al., 2017), this signaling may not directly control the elimination of the remaining PC dendrites via regulating the actin network. Consistently, the inhibition of N-WASP-Arp2/3 signaling did not hamper the elimination of the primitive apical PC dendrite after the fusiform cell stage, resulting in the cells forming a stellate cell-like shape (Fig. 3B,C,J; Figs S3B,C and S5). Therefore, N-WASP-Arp2/3 signaling likely plays a crucial role in the mechanism that selects and/or strengthens a single dendrite to become a stem dendrite, and inhibiting this signaling may cease PC development at the stellate cell stage because the system eliminating surplus dendrites may no longer be activated. Future studies aimed at unraveling the N-WASP-Arp2/3 signaling-mediated mechanism assigning a single stem dendrite are anticipated to facilitate our understanding of the principle in dendrite specification.

Upstream signals activating N-WASP-Arp2/3 during maturation of PC dendrites

Cdc42 is one of the key effectors in cytoskeletal organization induced by diverse extracellular signals including growth factors, guidance molecules, cytokines, trophic factors, G-protein coupled receptor (GPCR) ligands and proteoglycans via their receptors mainly categorized to receptor tyrosine kinases (RTKs) and GPCRs (Sinha and Yang, 2008). The defect in the early phase of PC dendrite maturation caused by N-WASP VCA was not restored by the co-expression of N-WASP H208D, which cannot bind to Cdc42, but was significantly restored by wild-type N-WASP (Fig. 4). This fact suggests that the mechanism of PC dendrite maturation through N-WASP-Arp2/3 signaling absolutely requires Cdc42 as an upstream regulator, and may therefore be mediated to

some extent by an extracellular signal(s). In support of this idea, the process of PC dendrite development in the dissociated culture and cerebellar slice culture, where extracellular signals in the cerebellum would have been disturbed, only partially recapitulates the *in vivo* situation; for example, many cells fail to completely reorganize their dendrites, thereby retaining multiple dendrites that are smaller than PCs *in vivo* even after long cultivation (Fig. 2D) (Fujishima et al., 2012). Thus, the extrinsic signals that are strictly regulated in time, space and quantity in the cerebellum, could potentially instruct the formation of a single stem dendrite via Cdc42-N-WASP-Arp2/3 signaling in PCs between P4 and P10. In the agranular cerebellum and the cerebellum of *weaver* mice, the cerebellar granule cells die owing to early postnatal X-irradiation or before migration, respectively (Sotelo, 1975, 1978). Because of this, PCs are unable to form a single stem dendrite and instead possess disoriented multiple short dendrites. Therefore, granule cells are thought to be the most potent source of extrinsic signals that direct PC dendrite formation (Sotelo and Dusart, 2009).

The brain-derived neurotrophic factor (BDNF) and its receptor TrkB (Ntrk2), an RTK, are expressed in both granule cells and PCs in the developing cerebellum. In addition, Cdc42 regulates actin dynamics downstream of BDNF-TrkB signaling to elicit spine maturation in hippocampal neurons and growth cone movement in retinal neurons (Chen et al., 2006; Shen et al., 2006). PCs in *Bdnf*-deficient mice at P8, when wild-type PCs start to enter the young PC stage, exhibit a severely atrophied morphology with multiple dendrites that randomly emanate from the cell body (Schwartz et al., 1997). Highly branched dendritic arbors were formed with a single stem dendrite at P24, albeit less extensive than the wild-type (Carter et al., 2002). Although the abnormality in the stem dendrite formation in *Bdnf*-deficient mice at P8 is resolved at the later stage, as described above, BDNF could possibly be the key extracellular signal that activates Cdc42-N-WASP-Arp2/3 signaling to establish a stem dendrite particularly between P4 and P10. In this case of *Bdnf*-deficient mice, BDNF deletion would prevent the formation of a stem dendrite during the correct period, but other extracellular signal(s) might activate Cdc42 to form a stem dendrite at the later stage. Indeed, various RTKs and their ligands, such as TrkC and NT-3, that potentially activate Cdc42 are expressed by developing PCs after P8 (Wüllner et al., 1998). Because the circulating T3, deficiency of which causes a striking interference in PC dendrite formation during the early phase of development (Vincent et al., 1982; Legrand, 1984), promotes the expression of BDNF and NT-3 in the cerebellum (Neveu and Arenas, 1996; Koibuchi et al., 1999), T3 may act as a further upstream signal for these neurotrophins to accomplish dendritic maturation in PCs via Cdc42-N-WASP-Arp2/3 signaling.

In addition, T3 reportedly elicits PC dendrite development via multiple downstream pathways. T3 induces the expression of PGC-1α, a master regulator of mitochondrial biogenesis, in PCs during cerebellar development. PGC-1α knockdown during the embryonic stage severely impairs the structure of PC dendrites with disoriented multiple short dendrites resembling PCs in the stellate cell stage (Hatsukano et al., 2017), similar to PCs expressing N-WASP VCA, PRDVCA or mem ΔVCA (Fig. 3B-J; Figs S3B,C and S5). However, the molecular correlation between PGC-1α and N-WASP-Arp2/3 signaling has not been clarified. Another T3 target is RORα, a nuclear receptor that participates in transcriptional regulation, which is induced in PCs as early as P0 (Boukhtouche et al., 2010). The *RORa* gene was originally identified as a responsible gene in *staggerer* mice (Hamilton et al., 1996). RORα is involved in various steps of development of PC dendrites including

the transition from the fusiform cell stage to stellate cell stage, stem dendrite formation and even spine maturation (Takeo et al., 2015). Although RORα knockdown in PCs from P4 causes a phenotype of multiple dendrites (Takeo et al., 2015), these dendrites are quite long and differ significantly in morphology from PCs expressing N-WASP VCA, PRDVCA or mem ΔVCA (Fig. 3B,C,J; Figs S3B,C and S5). Therefore, RORα may not be a direct upstream regulator of N-WASP-Arp2/3 signaling during stem dendrite formation in PCs. Nevertheless, as RORα targets the transcription of diverse genes in the cerebellum (Gold et al., 2003), RORα could be indirectly involved in N-WASP-Arp2/3 signaling through an unidentified transcriptional program for a set of genes modulating that signaling.

Altogether, temporally precise activation of Cdc42 and subsequent N-WASP-Arp2/3 signaling that might be, at least in part, directed by extrinsic signal(s) during cerebellar development may ensure stem dendrite formation at the appropriate time point and subsequent sufficient dendritic expansion. Continued work elucidating the upstream mechanisms of Cdc42-N-WASP-Arp2/3 signaling during cerebellar development will facilitate our understanding of an overall program that establishes a single stem dendrite in PCs.

MATERIALS AND METHODS
Animals
ICR (JAPAN SLC) mice were bred in the animal facility of Shimane University School of Medicine (Japan). All animal care and experimental procedures were performed in accordance with institutional guidelines approved by the Experimental Animal Care Committee of Shimane University School of Medicine. The day of confirmation of the vaginal plug was set as embryonic day (E) 0, and the day of birth was set as P0. Mice of both sexes were used for analyses.

Plasmids
The open reading frames (ORFs) of mouse *Arp3* and *N-WASP* were amplified using PCR from cDNA libraries of P4 and P12 mouse brains and cloned into pCAG-neo (WAKO). pAAV-L7-6-GFP-WPRE (Addgene plasmid #126462) (Nitta et al., 2017), pUCmini-iCAP-PHP.eB (Addgene plasmid #103005) (Chan et al., 2017) and pHelper (Agilent Technologies) were purchased. N-WASP truncates including VCA (385-501 amino acids), PRDVCA (274-501 amino acids), and ΔVCA (1-384 amino acids) were PCR amplified from pCAG-neo-N-WASP and cloned into the KpnI and SpeI sites of pCAG-neo. To construct pAAV-L7-6-HA-N-WASP PRDVCA-WPRE or pAAV-L7-6-mCherry-WPRE, GFP was excised from pAAV-L7-6-GFP-WPRE by digestion at the AgeI and NotI sites, and the PCR-amplified N-WASP PRDVCA or mCherry were cloned into those sites. N-WASP Y253E and H208D were constructed using KOD -Plus- Mutagenesis Kit (Toyobo). The hemagglutinin (HA) sequence was inserted into the 3′-end of the N-WASP ORFs. The membrane-anchored forms of N-WASP were constructed by insertion of the palmitoylation signal of growth associated protein 43 into the 5′-end of the ORFs. For the pCAG-neo vectors expressing mCherry-fused proteins, mCherry was cloned into the 5′-end of N-WASP wild-type or H208D and the 3′-end of *Arp3*.

Antibodies
The following primary antibodies were used for immunohistochemistry and immunocytochemistry: anti-N-WASP (rabbit, ab126626, Abcam, 1:200), anti-phospho-N-WASP (rabbit, PA5-105307, Invitrogen, 1:500), anti-Arp2 (mouse, sc-166103, Santa Cruz Biotechnology, 1:200), anti-Arp3 (mouse, A5979, Sigma-Aldrich, 1:400), anti-Cdc42 (mouse, ACD03, Cytoskeleton, 1:300), anti-calbindin (guinea pig, 214 004, Synaptic Systems, 1:1000), anti-GFP (chick, GFP-1010, Aves, 1:1000), anti-HA (rat, 11867423001, Roche, 1:2000), anti-RFP (rabbit, PM005, MBL, 1:500), anti-giantin (rabbit, PRB-114C, Covance, 1:1000). The following secondary antibodies from Jackson ImmunoResearch were used at 1:1000; Alexa Fluor 594-conjugated donkey anti-rabbit IgG (711-585-152), Alexa Fluor 594-conjugated donkey anti-mouse IgG (715-585-151), Alexa Fluor 488-conjugated donkey anti-guinea pig IgG (706-546-148), Alexa Fluor 488-conjugated donkey anti-chicken IgY (703-545-155), Alexa Fluor 594-conjugated goat anti-rat IgG (112-586-143), Alexa Fluor 647-conjugated donkey anti-rat IgG (712- 605-153), Alexa Fluor 488-conjugated goat anti-rat IgG (112-546-143).

In utero electroporation
In utero electroporation was performed as previously described (Kuwako et al., 2014; Kuwako and Okano, 2018), with some modifications. Briefly, pregnant mice at E12 were anesthetized with isoflurane (Pfizer) in an oxygenated carrier, and the uterus was externalized from the abdominal cavity. Plasmids used for electroporation were purified using NucleoBond Xtra midi kit (Macherey-Nagel) and dissolved in sterilized phosphate-buffered saline (PBS). A total of 1.0-2.0 μl of plasmid DNA containing 0.01% Fast Green (Sigma-Aldrich) in PBS was injected into the fourth ventricle with a glass capillary. An embryo was held with a forceps-type electrode (CUY650P3, Nepagene) and was electroporated through the uterine wall by NEPA21 electroporator (Nepagene) using the following settings: poring pulse: 40 V, 30 ms pulse length, 50 ms pulse interval, two pulses, 10% decay rate,+polarity; transfer pulse: 10 V, 50 ms pulse length, 50 ms pulse interval, three pulses, 40% decay rate,+polarity. After electroporation, the uterus was repositioned in the abdominal cavity and the abdominal wall and skin were closed, allowing the embryos to continue normal development. The plasmids used for *in utero* electroporation were as follows. Experiments for Venus expression alone (Fig. S3A): 1.0 μg of pCAG-Venus. Experiments for N-WASP mutant expression (Figs 3 and 5; Figs S3B, S4, S5, S7, S8): 5.0 μg of pCAG-neo and 1.0 μg of pCAG-Venus for control; 5.0 μg of pCAG-neo-HA-N-WASP wild-type/VCA/PRDVCA/ mem VCA/mem PRDVCA/Y253E/mem Y253E/mem ΔVCA and 1.0 μg of pCAG-Venus for N-WASP mutants. Rescue experiment (Fig. 4): 9.0 μg of pCAG-neo and 1.0 μg of pCAG-Venus for control; 4.5 μg of pCAG-neo, 4.5 μg of pCAG-neo-HA-N-WASP VCA and 1.0 μg of pCAG-Venus for N-WASP VCA without rescue, 4.5 μg of pCAG-neo mCherry N-WASP wild-type/H208D and 4.5 μg of pCAG-neo-HA-N-WASP VCA and 1.0 μg of pCAG-Venus for rescue by mCherry-fused N-WASP.

Immunohistochemistry
Immunohistochemistry was performed as described previously (Kuwako and Okano, 2018). Briefly, mice were transcardially perfused with 4% paraformaldehyde (PFA) in PBS (pH 7.4), and the brains were dissected and postfixed in 4% PFA in PBS overnight at 4°C. Tissue sections (60 μm thickness) were prepared using a vibratome (VT1000S, Leica). The sagittal floating sections were permeabilized with 0.3% Triton X-100 in PBS for 15 min at room temperature (RT), incubated with TNB blocking buffer (PerkinElmer) for 1 h at RT and subsequently incubated with primary antibodies in TNB blocking buffer overnight at 4°C, followed by incubation with secondary antibodies in TNB blocking buffer for 1.5 h at RT. For N-WASP, Arp2 and Cdc42-immunostaining, the floating sections were treated with 10 mM sodium citrate buffer (pH 6.0), for 30 min at 95°C using a BioShaker (Taitech) for antigen retrieval before permeabilization. A Vectastain Elite ABC kit (Vector Laboratories) and Tyramide Signal Amplification Plus Tetramethylrhodamine kit (PerkinElmer) were used for phospho-N-WASP-immunostaining. Nuclear DNA was detected with 10 μg/ml Hoechst 33342 (Dojindo). The images were acquired using fluorescence microscopes (FV1000, Olympus; BZ-X810, Keyence).

Immunocytochemistry
Primary PCs and NIH3T3 cells were fixed with 4% PFA in PBS (pH 7.4) for 15 min at 4°C, and then permeabilized with 0.3% Triton X-100 in PBS for 15 min at RT and incubated with TNB blocking buffer for 1 h at RT. Cells were then incubated with primary antibodies in TNB blocking buffer overnight at 4°C, followed by incubation with secondary antibodies in TNB blocking buffer for 1.5 h at RT. Nuclear DNA was detected with 10 μg/ml Hoechst 33342. The images were observed with a fluorescence microscope (BZ-X810, Keyence).

12

PC culture

The cerebella were dissected from E18 littermates in ice-cold Ca^{2+}/Mg^{2+}-free HBSS (Thermo Fisher Scientific) and dissociated with 0.375 mg/ml papain (Worthington). For pharmacological experiments, dissociated cells were resuspended in DMEM/F12 (Thermo Fisher Scientific) with 10% fetal bovine serum (FBS) (BioWest), plated on a 14 mm coverglass coated with 1 mg/ml poly-D-lysine (PDL) (Sigma-Aldrich) at a density of 1.0×10^6 cells per well in 24 well culture plate, and incubated for 3 h at $37°C/5\%$ CO_2. After incubation in DMEM/F12 with 10% FBS, the culture medium was replaced by DFB27 medium [DMEM/F12 containing 1% B27 supplement (Life Technologies), 0.6% glucose (Nacalai Tesque), 1.125 mg/ml $NaHCO_3$ (WAKO), 0.05 M HEPES (Sigma-Aldrich), 20 µg/ml insulin (Sigma-Aldrich), 100 µg/ml transferrin (Sigma-Aldrich), 30 nM sodium selenite (Sigma-Aldrich), 40 nM progesterone (Sigma-Aldrich), 10 µg/ml putrescine dihydrochloride (Sigma-Aldrich), 10 nM 3-iodo-L-tyrosine (Sigma-Aldrich), 2× GlutaMax (Thermo Fisher Scientific), 0.1 mg/ml bovine serum albumin (Nacalai Tesque), 1× penicillin (100 units/ml)/ streptomycin (100 µg/ml) (WAKO) and 3 µM cytosine β-D-arabinofuranoside hydrochloride (Sigma-Aldrich)]. Cells were maintained at $37°C/5\%$ CO_2 with partial replacement of the media every 4-7 days. For live cell imaging experiments, dissociated cells were resuspended in Opti-MEM (Thermo Fisher Scientific). Then $1.0\text{-}1.25 \times 10^6$ cells in 100 µl Opti-MEM with 7.5 µg pAAV-L7-6-GFP-WPRE and 7.5 µg pCAG-neo Arp3-mCherry were placed in an electrode cuvette (Nepagene). Cells were electroporated using a NEPA21 electroporator using the following settings: poring pulse: 150 V, 0.8 ms pulse length, 50 ms pulse interval, two pulses, 10% decay rate,+polarity; transfer pulse: 20 V, 50 ms pulse length, 50 ms pulse interval, five pulses, 40% decay rate,±polarity. After electroporation, cells were immediately resuspended in DFB27 medium with 10% FBS and plated on 1 mg/ml PDL-coated four-well-cover glass chamber (IWAKI) at a density of $2.0\text{-}2.5 \times 10^6$ cells per well and incubated at $37°C/5\%$ CO_2. After 3 h incubation, the culture medium was replaced by DFB27 medium.

Pharmacological experiments

N-WASP inhibitor wiskostatin (ab141085, Abcam), Arp2/3 inhibitor CK 666 (ab141231, Abcam), and Cdc42 GTPase inhibitor ML 141 (ab145603, Abcam) were dissolved in dimethyl sulfoxide (DMSO), diluted in culture medium and added to primary PCs throughout the duration of the culture at a final concentration of 1 µM, 50 µM and 10 µM, respectively. DMSO was used for control of inhibitors. The PC nuclei were visualized by Hoechst staining to assess the dying PCs with pyknotic nucleus.

Live cell imaging and data analysis

Time-lapse images of electroporated cells at 3-7 DIV were acquired at 3-10 min intervals for 12 h using a fluorescence microscope BZ-X810 (Keyence) equipped with a stage top temperature-controlled thermal plate [STR Model KIW(S/N990232), Tokai Hit]. During imaging, cells were maintained in an incubation chamber at $37°C/5\%$ CO_2 and the focus was auto-adjusted by the focus tracking mode of BZ-X810. The signal intensity of mCherry fluorescence was measured by software (BZ-H4M, Keyence) at the time point just before dendritic branching and the base points when the fluorescence signals were stable 2 min 25 s to 26 min 40 s before the aforementioned point.

Dendrite analysis

We analyzed lobes IV, V, VI, VII, VIII and IX of the cerebellum because of the consistency of the number of electroporated PCs in each brain and the identity of the phenotypes among those lobes. The entire morphology of dendrites was visualized by sparse PC labeling with Venus, and 0.3 µm-interval z-stack images were acquired with the z-stack mode of BZ-X810. The dendrites were traced and skeletonized in reconstructed z-stack images using Neurolucida 360 software (MBF Biosciences). Similarly, in pharmacological analysis *in vitro*, the dendrites were traced and skeletonized in two dimensional images using Neurolucida 360. The total dendrite length and number of branches were calculated on a skeletonized reconstruction using Neurolucida Explorer software (MBF Biosciences). The dendrite area was calculated using the convex-hull method with

Neurolucida Explorer. The branching frequency was calculated by dividing the total branch number by total dendrite length and converting the data to the number of branches per 100 µm. The orientation of dendrites was classified into three directions, apical, lateral and basal, as shown in the scheme in Fig. 3H, and PCs were divided into the three groups: (1) apical+basal+lateral, (2) apical+lateral and (3) apical. All the PCs that we analyzed fell into one of the three groups. To quantify the dendrite number, a dendrite was defined as the neurite(s), except for axon, that directly elongated from the cell body of PC. For dendrite height, as the width of the molecular layer varies from region to region within the cerebellar cortex, the distance from the cell body to the highest dendrite and the width of the molecular layer were measured, and dendrite height was calculated as a ratio to the height of the molecular layer. For the experimental results shown in Fig. 6B, dendrites with a height of less than 70% of the height of the molecular layer were defined as abnormal.

Transfection into NIH3T3 cells

NIH3T3 cells were maintained in DMEM with 10% FBS and transfected with 8.0 µg of pCAG-neo-HA-N-WASP VCA, mem VCA, PRDVCA or mem PRDVCA using a NEPA21 electroporator. The cells were fixed 48 h later for immunocytochemistry.

AAV production and injection

Recombinant AAV vectors were produced by HEK293T cells (GenHunter) transfected with viral DNAs including pAAV-L7-6-HA-N-WASP PRDVCA-WPRE, pUCmini-iCAP-PHP.eB and pHelper, as described previously (Konno and Hirai, 2020). HEK293T cells were cultured in a 10 cm dish with DMEM (Sigma-Aldrich) supplemented with 10% FBS, and transfected with viral vectors using the polyethylenimine method using PEI MAX (Polysciences). The transfection reagent-containing culture medium was replaced with serum-free DMEM at 24 h post-transfection. After 5 days from medium change, AAV-containing medium was collected and concentrated using Pierce Protein Concentrator PES, 100K MWCO, 5-20 ml (Thermo Fisher Scientific). The final volume of AAV solution was ∼200-500 µl. The viral genomic titer was measured by real-time quantitative PCR using the extracted viral genomic DNA from the concentrated viral solution and Thunderbird SYBR qPCR Mix (Toyobo) with the primers for WPRE sequences being 5′-CTGTTGGGCACTGACAATTC-3′ and 5′-GAAGGGACGTAGCAGAAGGA-3′. The PCR reaction parameters were an initial denaturation phase of $95°C$ for 1 min, two-step PCR phase of $95°C$ for 15 s, $60°C$ for 30 s (40 cycles). For viral transduction in ICR mouse at P7, 100 µl of the viral solution mixture (AAV-L7-6-HA-N-WASP PRDVCA; 4.0×10^{12} viral genome, AAV-L7-6-mCherry; 8.0×10^9 viral genome) was intravenously injected into the retro-orbital sinus of mice using a 0.5 ml syringe with a 30-gauge needle (Nipro).

DEVELOPMENT

13

Peer review history
The peer review history is available online at https://journals.biologists.com/dev/lookup/doi/10.1242/dev.201214.reviewer-comments.pdf

References

Alvarez-Saavedra, M., De Repentigny, Y., Lagali, P. S., Raghu Ram, E. V. S., Yan, K., Hashem, E., Ivanochko, D., Huh, M. S., Yang, D., Mears, A. J. et al. (2014). Snf2h-mediated chromatin organization and histone H1 dynamics govern cerebellar morphogenesis and neural maturation. *Nat. Commun.* **5**, 4181. doi:10.1038/ncomms5181

Armengol, J.-A. and Sotelo, C. (1991). Early dendritic development of Purkinje cells in the rat cerebellum. A light and electron microscopic study using axonal tracing in 'in vitro' slices. *Brain Res. Dev. Brain Res.* **64**, 95-114. doi:10.1016/0165-3806(91)90213-3

Boukhtouche, F., Janmaat, S., Vodjdani, G., Gautheron, V., Mallet, J., Dusart, I. and Mariani, J. (2006). Retinoid-related orphan receptor α controls the early steps of Purkinje cell dendritic differentiation. *J. Neurosci.* **26**, 1531-1538. doi:10.1523/JNEUROSCI.4636-05.2006

Boukhtouche, F., Brugg, B., Wehrlé, R., Bois-Joyeux, B., Danan, J.-L., Dusart, I. and Mariani, J. (2010). Induction of early Purkinje cell dendritic differentiation by thyroid hormone requires RORα. *Neural Dev.* **5**, 18. doi:10.1186/1749-8104-5-18

Brodbeck, J., Davies, A., Courtney, J.-M., Meir, A., Balaguero, N., Canti, C., Moss, F. J., Page, K. M., Pratt, W. S., Hunt, S. P. et al. (2002). The ducky mutation in Cacna2d2 results in altered Purkinje cell morphology and is associated with the expression of a truncated alpha 2 delta-2 protein with abnormal function. *J. Biol. Chem.* **277**, 7684-7693. doi:10.1074/jbc.M109404200

Carter, A. R., Chen, C., Schwartz, P. M. and Segal, R. A. (2002). Brain-derived neurotrophic factor modulates cerebellar plasticity and synaptic ultrastructure. *J. Neurosci.* **22**, 1316-1327. doi:10.1523/JNEUROSCI.22-04-01316.2002

Chacón, M. R., Navarro, A. I., Cuesto, G., del Pino, I., Scott, R., Morales, M. and Rico, B. (2012). Focal adhesion kinase regulates actin nucleation and neuronal filopodia formation during axonal growth. *Development* **139**, 3200-3210. doi:10.1242/dev.080564

Chan, K. Y., Jang, M. J., Yoo, B. B., Greenbaum, A., Ravi, N., Wu, W.-L., Sánchez-Guardado, L., Lois, C., Mazmanian, S. K., Deverman, B. E. et al. (2017). Engineered AAVs for efficient noninvasive gene delivery to the central and peripheral nervous systems. *Nat. Neurosci.* **20**, 1172-1179. doi:10.1038/nn.4593

Chen, T.-J., Gehler, S., Shaw, A. E., Bamburg, J. R. and Letourneau, P. C. (2006). Cdc42 participates in the regulation of ADF/cofilin and retinal growth cone filopodia by brain derived neurotrophic factor. *J. Neurobiol.* **66**, 103-114. doi:10.1002/neu.20204

Dharmalingam, E., Haeckel, A., Pinyol, R., Schwintzer, L., Koch, D., Kessels, M. M. and Qualmann, B. (2009). F-BAR proteins of the syndapin family shape the plasma membrane and are crucial for neuromorphogenesis. *J. Neurosci.* **29**, 13315-13327. doi:10.1523/JNEUROSCI.3973-09.2009

Fujishima, K., Horie, R., Mochizuki, A. and Kengaku, M. (2012). Principles of branch dynamics governing shape characteristics of cerebellar Purkinje cell dendrites. *Development* **139**, 3442-3455. doi:10.1242/dev.081234

Fukumitsu, K., Hatsukano, T., Yoshimura, A., Heuser, J., Fujishima, K. and Kengaku, M. (2016). Mitochondrial fission protein Drp1 regulates mitochondrial transport and dendritic arborization in cerebellar Purkinje cells. *Mol. Cell Neurosci.* **71**, 56-65. doi:10.1016/j.mcn.2015.12.006

Ganeshan, R., Nowotarski, K., Di, A., Nelson, D. J. and Kirk, K. L. (2006). CFTR surface expression and chloride currents are decreased by inhibitors of N-WASP and actin polymerization. *Biochim. Biophys. Acta* **1773**, 192-200. doi:10.1016/j.bbamcr.2006.09.031

Gao, Y., Perkins, E. M., Clarkson, Y. L., Tobia, S., Lyndon, A. R., Jackson, M. and Rothstein, J. D. (2011). beta-III spectrin is critical for development of purkinje cell dendritic tree and spine morphogenesis. *J. Neurosci.* **31**, 16581-16590. doi:10.1523/JNEUROSCI.3332-11.2011

Gibson, D. A., Tymanskyj, S., Yuan, R. C., Leung, H. C., Lefebvre, J. L., Sanes, J. R., Chédotal, A. and Ma, L. (2014). Dendrite self-avoidance requires cell-autonomous slit/robo signaling in cerebellar purkinje cells. *Neuron* **81**, 1040-1056. doi:10.1016/j.neuron.2014.01.009

Gold, D. A., Baek, S. H., Schork, N. J., Rose, D. W., Larsen, D. L. D., Sachs, B. D., Rosenfeld, M. G. and Hamilton, B. A. (2003). RORα coordinates reciprocal signaling in cerebellar development through sonic hedgehog and calcium-dependent pathways. *Neuron* **40**, 1119-1131. doi:10.1016/S0896-6273(03)00769-4

Hamilton, B. A., Frankel, W. N., Kerrebrock, A. W., Hawkins, T. L., FitzHugh, W., Kusumi, K., Russell, L. B., Mueller, K. L., van Berkel, V., Birren, B. W. et al. (1996). Disruption of the nuclear hormone receptor RORalpha in staggerer mice. *Nature* **379**, 736-739. doi:10.1038/379736a0

Hasegawa, K. and Kuwako, K.-I. (2022). Molecular mechanisms regulating the spatial configuration of neurites. *Semin. Cell Dev. Biol.* **129**, 103-114. doi:10.1016/j.semcdb.2022.02.015

Hatsukano, T., Kurisu, J., Fukumitsu, K., Fujishima, K. and Kengaku, M. (2017). Thyroid hormone induces PGC-1α during dendritic outgrowth in mouse cerebellar purkinje cells. *Front. Cell. Neurosci.* **11**, 133. doi:10.3389/fncel.2017.00133

Irie, F. and Yamaguchi, Y. (2002). EphB receptors regulate dendritic spine development via intersectin, Cdc42 and N-WASP. *Nat. Neurosci.* **5**, 1117-1118. doi:10.1038/nn964

Jain, N., Lim, L. W., Tan, W. T., George, B., Makeyev, E. and Thanabalu, T. (2014). Conditional N-WASP knockout in mouse brain implicates actin cytoskeleton regulation in hydrocephalus pathology. *Exp. Neurol.* **254**, 29-40. doi:10.1016/j.expneurol.2014.01.011

Joo, W., Hippenmeyer, S. and Luo, L. (2014). Neurodevelopment. Dendrite morphogenesis depends on relative levels of NT-3/TrkC signaling. *Science* **346**, 626-629. doi:10.1126/science.1258990

Kakimoto, T., Katoh, H. and Negishi, M. (2006). Regulation of neuronal morphology by Toca-1, an F-BAR/EFC protein that induces plasma membrane invagination. *J. Biol. Chem.* **281**, 29042-29053. doi:10.1074/jbc.M604025200

Kawabata Galbraith, K., Fujishima, K., Mizuno, H., Lee, S.-J., Uemura, T., Sakimura, K., Mishina, M., Watanabe, N. and Kengaku, M. (2018). MTSS1 regulation of actin-nucleating formin DAAM1 in dendritic filopodia determines final dendritic configuration of Purkinje cells. *Cell Rep.* **24**, 95-106.e109. doi:10.1016/j.celrep.2018.06.013

Kessels, M. M., Schwintzer, L., Schlobinski, D. and Qualmann, B. (2011). Controlling actin cytoskeletal organization and dynamics during neuronal morphogenesis. *Eur. J. Cell Biol.* **90**, 926-933. doi:10.1016/j.ejcb.2010.08.011

King, S. J., Worth, D. C., Scales, T. M. E., Monypenny, J., Jones, G. E. and Parsons, M. (2011). β1 integrins regulate fibroblast chemotaxis through control of N-WASP stability. *EMBO J.* **30**, 1705-1718. doi:10.1038/emboj.2011.82

Koibuchi, N., Fukuda, H. and Chin, W. W. (1999). Promoter-specific regulation of the brain-derived neurotropic factor gene by thyroid hormone in the developing rat cerebellum. *Endocrinology* **140**, 3955-3961. doi:10.1210/endo.140.9.6997

Konietzny, A., Bär, J. and Mikhaylova, M. (2017). Dendritic actin cytoskeleton: structure, functions, and regulations. *Front. Cell. Neurosci.* **11**, 147. doi:10.3389/fncel.2017.00147

Konno, A. and Hirai, H. (2020). Efficient whole brain transduction by systemic infusion of minimally purified AAV-PHP.eB. *J. Neurosci. Methods* **346**, 108914. doi:10.1016/j.jneumeth.2020.108914

Korobova, F. and Svitkina, T. (2008). Arp2/3 complex is important for filopodia formation, growth cone motility, and neuritogenesis in neuronal cells. *Mol. Biol. Cell* **19**, 1561-1574. doi:10.1091/mbc.e07-09-0964

Kurisu, S. and Takenawa, T. (2009). The WASP and WAVE family proteins. *Genome Biol.* **10**, 226. doi:10.1186/gb-2009-10-6-226

Kuwako, K.-I. and Okano, H. (2018). The LKB1-SIK pathway controls dendrite self-avoidance in Purkinje cells. *Cell Rep.* **24**, 2808-2818.e2804. doi:10.1016/j.celrep.2018.08.029

Kuwako, K. I., Nishimoto, Y., Kawase, S., Okano, H. J. and Okano, H. (2014). Cadherin-7 regulates mossy fiber connectivity in the cerebellum. *Cell Rep.* **9**, 311-323. doi:10.1016/j.celrep.2014.08.063

Landis, D. M. D. and Sidman, R. L. (1978). Electron microscopic analysis of postnatal histogenesis in the cerebellar cortex of staggerer mutant mice. *J. Comp. Neurol.* **179**, 831-863. doi:10.1002/cne.901790408

Larramendi, L. M. (1969). Analysis of synaptogenesis in the cerebellum of the mouse. In *Neurobiology of Cerebellar Evolution and Development* (ed. R. Llinas), pp. 803-843. Chicago: American Medical Association.

Lefebvre, J. L., Kostadinov, D., Chen, W. V., Maniatis, T. and Sanes, J. R. (2012). Protocadherins mediate dendritic self-avoidance in the mammalian nervous system. *Nature* **488**, 517-521. doi:10.1038/nature11305

Legrand, J. (1984). Effects of thyroid hormones on central nervous system. In *Neurobehavioural teratology* (ed. J. Yanai), pp. 331-363. Amsterdam: Elsevier/North Holland.

Li, J., Gu, X., Ma, Y., Calicchio, M. L., Kong, D., Teng, Y. D., Yu, L., Crain, A. M., Vartanian, T. K., Pasqualini, R. et al. (2010). Nna1 mediates Purkinje cell dendritic development via lysyl oxidase propeptide and NF-kappaB signaling. *Neuron* **68**, 45-60. doi:10.1016/j.neuron.2010.08.013

Li, J., Yu, L., Gu, X., Ma, Y., Pasqualini, R., Arap, W., Snyder, E. Y. and Sidman, R. L. (2013). Tissue plasminogen activator regulates Purkinje neuron development and survival. *Proc. Natl. Acad. Sci. USA* **110**, E2410-E2419. doi:10.1073/pnas.1305010110

Liu, R., Xu, M., Zhang, X.-Y., Zhou, M.-J., Zhou, B.-Y., Qi, C., Song, B., Fan, Q., You, W.-Y., Zhu, J.-N. et al. (2020). PDK1 regulates the maintenance of cell body and the development of dendrites of Purkinje cells by pS6 and PKCγ. *J. Neurosci.* **40**, 5531-5548. doi:10.1523/JNEUROSCI.2496-19.2020

Luck, R., Karakatsani, A., Shah, B., Schermann, G., Adler, H., Kupke, J., Tisch, N., Jeong, H.-W., Back, M. K., Hetsch, F. et al. (2021). The angiopoietin-Tie2 pathway regulates Purkinje cell dendritic morphogenesis in a cell-autonomous manner. *Cell Rep.* **36**, 109522. doi:10.1016/j.celrep.2021.109522

Luo, L. (2021). Architectures of neuronal circuits. *Science* **373**, eabg7285. doi:10.1126/science.abg7285

DEVELOPMENT

Machesky, L. M. and Insall, R. H. (1998). Scar1 and the related Wiskott-Aldrich syndrome protein, WASP, regulate the actin cytoskeleton through the Arp2/3 complex. *Curr. Biol.* **8**, 1347-1356. doi:10.1016/S0960-9822(98)00015-3

Magdalena, J., Millard, T. H., Etienne-Manneville, S., Launay, S., Warwick, H. K. and Machesky, L. M. (2003). Involvement of the Arp2/3 complex and Scar2 in Golgi polarity in scratch wound models. *Mol. Biol. Cell* **14**, 670-684. doi:10.1091/mbc.e02-06-0345

Miki, H., Miura, K. and Takenawa, T. (1996). N-WASP, a novel actin-depolymerizing protein, regulates the cortical cytoskeletal rearrangement in a PIP2-dependent manner downstream of tyrosine kinases. *EMBO J.* **15**, 5326-5335. doi:10.1002/j.1460-2075.1996.tb00917.x

Miki, H., Sasaki, T., Takai, Y. and Takenawa, T. (1998). Induction of filopodium formation by a WASP-related actin-depolymerizing protein N-WASP. *Nature* **391**, 93-96. doi:10.1038/34208

Neveu, I. and Arenas, E. (1996). Neurotrophins promote the survival and development of neurons in the cerebellum of hypothyroid rats in vivo. *J. Cell Biol.* **133**, 631-646. doi:10.1083/jcb.133.3.631

Nitta, K., Matsuzaki, Y., Konno, A. and Hirai, H. (2017). Minimal Purkinje cell-specific PCP2/L7 promoter virally available for rodents and non-human primates. *Mol. Ther. Methods Clin. Dev.* **6**, 159-170. doi:10.1016/j.omtm.2017.07.006

Nolen, B. J., Tomasevic, N., Russell, A., Pierce, D. W., Jia, Z., McCormick, C. D., Hartman, J., Sakowicz, R. and Pollard, T. D. (2009). Characterization of two classes of small molecule inhibitors of Arp2/3 complex. *Nature* **460**, 1031-1034. doi:10.1038/nature08231

Peterson, J. R., Bickford, L. C., Morgan, D., Kim, A. S., Ouerfelli, O., Kirschner, M. W. and Rosen, M. K. (2004). Chemical inhibition of N-WASP by stabilization of a native autoinhibited conformation. *Nat. Struct. Mol. Biol.* **11**, 747-755. doi:10.1038/nsmb796

Pinyol, R., Haeckel, A., Ritter, A., Qualmann, B. and Kessels, M. M. (2007). Regulation of N-WASP and the Arp2/3 complex by Abp1 controls neuronal morphology. *PLoS ONE* **2**, e400. doi:10.1371/journal.pone.0000400

Pollard, T. D. and Borisy, G. G. (2003). Cellular motility driven by assembly and disassembly of actin filaments. *Cell* **112**, 453-465. doi:10.1016/S0092-8674(03)00120-X

Rohatgi, R., Ma, L., Miki, H., Lopez, M., Kirchhausen, T., Takenawa, T. and Kirschner, M. W. (1999). The interaction between N-WASP and the Arp2/3 complex links Cdc42-dependent signals to actin assembly. *Cell* **97**, 221-231. doi:10.1016/S0092-8674(00)80732-1

San Miguel-Ruiz, J. E. and Letourneau, P. C. (2014). The role of Arp2/3 in growth cone actin dynamics and guidance is substrate dependent. *J. Neurosci.* **34**, 5895-5908. doi:10.1523/JNEUROSCI.0672-14.2014

Schwartz, P. M., Borghesani, P. R., Levy, R. L., Pomeroy, S. L. and Segal, R. A. (1997). Abnormal cerebellar development and foliation in BDNF−/− mice reveals a role for neurotrophins in CNS patterning. *Neuron* **19**, 269-281. doi:10.1016/S0896-6273(00)80938-1

Serrano-Pertierra, E., Cernuda-Morollón, E. and López-Larrea, C. (2012). Wiskott-Aldrich syndrome protein (WASp) and N-WASp are involved in the regulation of NK-cell migration upon NKG2D activation. *Eur. J. Immunol.* **42**, 2142-2151. doi:10.1002/eji.201142070

Shen, W., Wu, B., Zhang, Z., Dou, Y., Rao, Z.-R., Chen, Y.-R. and Duan, S. (2006). Activity-induced rapid synaptic maturation mediated by presynaptic cdc42 signaling. *Neuron* **50**, 401-414. doi:10.1016/j.neuron.2006.03.017

Sinha, S. and Yang, W. (2008). Cellular signaling for activation of Rho GTPase Cdc42. *Cell Signal.* **20**, 1927-1934. doi:10.1016/j.cellsig.2008.05.002

Soha, J. M. and Herrup, K. (1995). Stunted morphologies of cerebellar Purkinje cells in lurcher and staggerer mice are cell-intrinsic effects of the mutant genes. *J. Comp. Neurol.* **357**, 65-75. doi:10.1002/cne.903570107

Sotelo, C. (1975). Anatomical, physiological and biochemical studies of the cerebellum from mutant mice. II. Morphological study of cerebellar cortical neurons and circuits in the weaver mouse. *Brain Res.* **94**, 19-44. doi:10.1016/0006-8993(75)90874-4

Sotelo, C. (1978). Purkinje cell ontogeny: formation and maintenance of spines. *Prog. Brain Res.* **48**, 149-170. doi:10.1016/S0079-6123(08)61021-3

Sotelo, C. and Dusart, I. (2009). Intrinsic versus extrinsic determinants during the development of Purkinje cell dendrites. *Neuroscience* **162**, 589-600. doi:10.1016/j.neuroscience.2008.12.035

Spillane, M., Ketschek, A., Jones, S. L., Korobova, F., Marsick, B., Lanier, L., Svitkina, T. and Gallo, G. (2011). The actin nucleating Arp2/3 complex contributes to the formation of axonal filopodia and branches through the regulation of actin patch precursors to filopodia. *Dev. Neurobiol.* **71**, 747-758. doi:10.1002/dneu.20907

Spillane, M., Ketschek, A., Donnelly, C. J., Pacheco, A., Twiss, J. L. and Gallo, G. (2012). Nerve growth factor-induced formation of axonal filopodia and collateral branches involves the intra-axonal synthesis of regulators of the actin-nucleating Arp2/3 complex. *J. Neurosci.* **32**, 17671-17689. doi:10.1523/JNEUROSCI.1079-12.2012

Strasser, G. A., Rahim, N. A., VanderWaal, K. E., Gertler, F. B. and Lanier, L. M. (2004). Arp2/3 is a negative regulator of growth cone translocation. *Neuron* **43**, 81-94. doi:10.1016/j.neuron.2004.05.015

Stürner, T., Tatarnikova, A., Mueller, J., Schaffran, B., Cuntz, H., Zhang, Y., Nemethova, M., Bogdan, S., Small, V. and Tavosanis, G. (2019). Transient localization of the Arp2/3 complex initiates neuronal dendrite branching in vivo. *Development* **146**, dev171397. doi:10.1242/dev.171397

Suetsugu, S., Hattori, M., Miki, H., Tezuka, T., Yamamoto, T., Mikoshiba, K. and Takenawa, T. (2002). Sustained activation of N-WASP through phosphorylation is essential for neurite extension. *Dev. Cell* **3**, 645-658. doi:10.1016/S1534-5807(02)00324-6

Surviladze, Z., Waller, A., Strouse, J. J., Bologa, C., Ursu, O., Salas, V., Parkinson, J. F., Phillips, G. K., Romero, E., Wandinger-Ness, A. et al. (2010). A potent and selective inhibitor of Cdc42 GTPase. In *Probe Reports from the NIH Molecular Libraries Program*. Bethesda, MD, PMID: 21433396.

Takeo, Y. H., Kakegawa, W., Miura, E. and Yuzaki, M. (2015). RORα regulates multiple aspects of dendrite development in cerebellar Purkinje cells in vivo. *J. Neurosci.* **35**, 12518-12534. doi:10.1523/JNEUROSCI.0075-15.2015

Takeo, Y. H., Shuster, S. A., Jiang, L., Hu, M. C., Luginbuhl, D. J., Rulicke, T., Contreras, X., Hippenmeyer, S., Wagner, M. J., Ganguli, S. et al. (2021). GluD2- and Cbln1-mediated competitive interactions shape the dendritic arbors of cerebellar Purkinje cells. *Neuron* **109**, 629-644.e628. doi:10.1016/j.neuron.2020.11.028

Tanabe, K., Kani, S., Shimizu, T., Bae, Y.-K., Abe, T. and Hibi, M. (2010). Atypical protein kinase C regulates primary dendrite specification of cerebellar Purkinje cells by localizing Golgi apparatus. *J. Neurosci.* **30**, 16983-16992. doi:10.1523/JNEUROSCI.3352-10.2010

Vincent, J., Legrand, C., Rabie, A. and Legrand, J. (1982). Effects of thyroid hormone on synaptogenesis in the molecular layer of the developing rat cerebellum. *J. Physiol. (Paris)* **78**, 729-738.

Wang, P.-S., Chou, F.-S., Ramachandran, S., Xia, S., Chen, H.-Y., Guo, F., Suraneni, P., Maher, B. J. and Li, R. (2016). Crucial roles of the Arp2/3 complex during mammalian corticogenesis. *Development* **143**, 2741-2752. doi:10.1242/dev.130542

Wegner, A. M., Nebhan, C. A., Hu, L., Majumdar, D., Meier, K. M., Weaver, A. M. and Webb, D. J. (2008). N-wasp and the arp2/3 complex are critical regulators of actin in the development of dendritic spines and synapses. *J. Biol. Chem.* **283**, 15912-15920. doi:10.1074/jbc.M801555200

Weiss, G. M. and Pysh, J. J. (1978). Evidence for loss of Purkinje cell dendrites during late development: a morphometric Golgi analysis in the mouse. *Brain Res.* **154**, 219-230. doi:10.1016/0006-8993(78)90696-0

Willig, K. I., Steffens, H., Gregor, C., Herholt, A., Rossner, M. J. and Hell, S. W. (2014). Nanoscopy of filamentous actin in cortical dendrites of a living mouse. *Biophys. J.* **106**, L01-L03. doi:10.1016/j.bpj.2013.11.1119

Wüllner, U., Isenmann, S., Gleichmann, M., Klockgether, T. and Bähr, M. (1998). Expression of neurotrophins and neurotrophin receptors in the cerebellum of mutant weaver and lurcher mice. *Brain Res. Dev. Brain Res.* **110**, 1-6. doi:10.1016/S0165-3806(98)00079-0

Yoshimura, T., Arimura, N. and Kaibuchi, K. (2006). Signaling networks in neuronal polarization. *J. Neurosci.* **26**, 10626-10630. doi:10.1523/JNEUROSCI.3824-06.2006

Zhang, S.-X., Duan, L.-H., He, S.-J., Zhuang, G.-F. and Yu, X. (2017). Phosphatidylinositol 3,4-bisphosphate regulates neurite initiation and dendrite morphogenesis via actin aggregation. *Cell Res.* **27**, 253-273. doi:10.1038/cr.2017.13